Published in : Journal of Constructional Steel Research (2022), vol. 192, 107215
DOI: 10.1016/j.jcsr.2022.107215
Status : Postprint (Author's version)

DROP-WEIGHT IMPACT TESTS ON FREE FROM DAMAGE BEAM TO COLUMN CONNECTIONS

M. D'Antimo[a], M. Latour[b], J.F. Demonceau[a]

[a] *University of Liège, UEE Department, Belgium*

[b] *University of Salerno, Department of Civil Engineering, Italy*

Keywords:

Drop-weight, SHJs, Impact, ABAQUS, DIFs, Strain rate, Mass impact tests, Dynamic loading

Abstract

Modern standards require the design of resilient structures, highlighting the need for systems able to assure life safety and an easy repairability. Indeed, a resilient design includes the conception and the realization of a structure able to sustain accidental or exceptional events with limited and easy-to-repair damages. Within this framework, steel Moment Resisting Frames (MRFs) equipped with Slide Hinge Joints, have proved to be extremely efficient for the seismic performance and damage avoidance. However, to date, limited knowledge exists on their behaviour under exceptional events and significant research efforts are still required.

In order to provide a contribution to fill this gap, this paper focuses on the behaviour of SHJs with Symmetric Friction Dampers (SFDs) under drop-weight impact. SHJs are normally designed to act as the dissipative fuse of MRFs under seismic loadings. However, they can be also effectively exploited to improve the robustness of steel buildings through the increase of the local ductility, which may ensure also the activation of catenary effects in beams and tying forces.

The response of MRFs equipped with such a joint under extreme dynamic loading condition is not straightforward. It requires a deep knowledge of their behaviour as a function of the strain rate. In this paper the results of six drop weight impact tests on double-sided SHJs are presented and a 3D finite element model is developed in ABAQUS software. A parametric analysis is then performed to investigate the influence of the key parameters affecting the joint behaviour, namely: the impact velocity, the impact mass and the impact energy.

In order to characterize the joint behaviour under impact, the paper provides a correlation between the dissipation rate of the joint, under impact, and the input energy. The work is limited to a geometric range and to the joint typology here considered, however, the methodology and the results can be generalized.

Published in : Journal of Constructional Steel Research (2022), vol. 192, 107215
DOI: 10.1016/j.jcsr.2022.107215
Status : Postprint (Author's version)

Overall, the joints perform better under higher velocities rather than higher masses due to strain rate effects. However, a clear correlation between the DIF and the velocity of rotation of the joint is difficult to establish.

1. Introduction

Connections are critical components of buildings, especially when robustness and integrity of structural systems is under concern. A localized failure at the level of a connection can compromise the local and the global stability of a structure. For these reasons, research of the last decades has strongly focused on the behaviour of joints and on the influence of the moment-rotation behaviour on the structural response. Joints able to provide high rotational capacity, such as the Sliding Hinge Joint (SHJ), represent promising solutions for the improvement of the robustness of steel structures. The intrinsic capacity to accommodate large rotations makes them particularly suitable for the activation of alternative load paths in structures under exceptional events such as the loss of a column [1]. In general, energy dissipaters have demonstrated to be a good option to build earthquake resistant structures [2] absorbing input seismic energy and achieving a free from damage structure [1,61,62,3].

SH joints have been initially proposed by Grigorian et al. [4] and the researchers of the Auckland University 2005 [5] using the proposed solution as seismic dampers in Moment Resisting steel Frames (MRFs). Other authors have investigated the benefit of these connections examining extensively their seismic performance [3,6–9]. Sliding Hinge Joints have been recognized as effective solutions to reduce the building repairing costs in case of destructive seismic events, ensuring large energy dissipation capacity with negligible damage. The slip resistance of a SHJ is usually provided by an Asymmetrical or a Symmetrical Friction Dampers (AFD or SFD), whose response depends on the friction coefficient of friction shims and the bolt preloading.

In [1,3] the friction damper has been realized with angles and a haunch bolted both to the bottom beam flange and to the column. The main benefit of this configuration is the possibility of prefabricating the damper, ensuring better control on the friction material and the correct application of the bolt tightening procedures in the shop. In **Fig. 1**, an example of a SHJ with a friction damper located at the bottom beam flange is presented.

Under serviceability limit state conditions, the connection is slip- resistant. In fact, between the haunch and the angles, friction pads coated with specific coatings investigated in [10], are designed to develop the required slip-resistance activating the dissipation through stable hysteretic loops only when the connection is subjected to severe seismic actions. The two main parameters governing the connection resistance are the bolt preloading and the friction coefficient, both have to be controlled to properly govern the damper resistance. To assess the friction damper properties, different coating materials have been investigated in previous works [10,11] under cyclic and impact loading conditions, providing the relevant values of the design friction coefficient and showing the effect of strain rate over the response of a friction damper. Additionally, further works have focused on the monitoring of the bolt preloading forces over time showing how the problem of initial loss of pretension can be addressed in design through the adoption of proper safety factors [12].

Published in : Journal of Constructional Steel Research (2022), vol. 192, 107215
DOI: 10.1016/j.jcsr.2022.107215
Status : Postprint (Author's version)

Design procedures for SHJs under seismic loading conditions, after several decades of research, are now well-established [6]. Contrarily, the behaviour of these joints subjected to accidental or exceptional events (e.g. impact, column loss, blast, etc.), has almost never been considered. Currently, even though these structures start to count a rather large number of practical applications [13], there are no design guidelines addressing the specificities related to the behaviour of MRFs equipped with SHJs subjected to exceptional loading events.

More in general, despite the growth of international research on structural robustness [14–20,63] and progressive collapse mitigation [21–25], only few design guidelines, as well as univocal and clear code recommendations, are nowadays available. Among the authors who investigated the impact or, more generically, the dynamic behaviour of joints/joint components [26–28], the dynamic behaviour of t-stubs under impact loads has been investigated in [29], as well as the friction damper behaviour in [30], providing a preliminary analytical procedure to predict the behaviour under high rate of deformation, based on the extension of the component method. The behaviour of joints under impact loading has also been investigated using experimental approaches. Grimsmo et al. [28] performed tests impacting axially the column of a cruciform beam-to-column joint (Gravitational dynamic loads) while Rahbari et al. [31] and Kang et al. [32] performed lateral impact tests, impacting the column orthogonally to the main axis. Impact tests performed using dropping masses have been carried out in [33–36].

However, it was evidenced by many authors that the results of the different experimental campaigns are often contradictory. For instance, in [37], the tests on extended end-plates shown an increase of ductility while, in [38], a decrease of ductility for similar connections has been found. The limited amount of data and the contradictories of some of the results, highlight the need for further investigations in this field.

More recently several testing campaigns have been carried out. In [39] the authors investigate the falling floor scenario of a steel frame with five different joint typologies identifying different energy dissipation capacities. Wang et al. in [40] provides tests extended up to failure of welded flange-bolted connections with three types of weld access holes under impact loadings underlining the importance of Finite element modelling and the difficulty to generalise the results.

In [41] the authors performed static and impact tests on fin plate and welded unreinforced flanges with bolted web joints and the model the test in LS-DYNA to extend the experimental campaign.

Both works [40,41] were performed using a dropping hammer on scaled specimens and classifying the behaviour using deformation ratio or energy dissipation.

The available studies dealing with the response of beam-to-column joints under impact loads are usually limited by the difficulty and the cost of executing real scale experimental tests. Many authors have recognized the benefit of using numerical modelling to complement the results of experimental campaigns [42]. Finite element modelling has proved to be a valid and reliable tool to cope with limited test data availability. It provides the possibility to observe the detailed evolution of the forces, stresses, deformations, strain rates, etc., which is not easy to measure during experimental tests. However, the complexity of FE modelling of connections under impact arises from the difficulty to model precisely material damage [43–45], strain rate and dynamic effects [28,31,37,46], which can lead to convergence

Published in : Journal of Constructional Steel Research (2022), vol. 192, 107215
DOI: 10.1016/j.jcsr.2022.107215
Status : Postprint (Author's version)

problem and increase of the time of analysis. Especially, the correct modelling of the materials, accounting for strain rate sensitivity, needs the calibration of different parameters. How to include these aspects in FE modelling has been already investigated by the same authors in [47], where the applicability of different methods has been examined providing basic parameters for the implementation of the semi-empirical Johnson-Cook law for commercial types of steel.

Within this framework, to provide an advancement to the research related to the behaviour of steel joints under impact loading conditions, this paper presents experimental impact tests on SHJ joints and their interpretation. Based on the obtained results, a 3D finite element model, including damage and strain rate effects is validated and used for parametric studies. Finally, the procedure to determine impact force and the DIF (Dynamic Increase Factor), following a similar approach used in [47] is extended to the tested joints. This paper shows the results of impact tests on SHJs to experimentally and numerically study the performance under dynamic events in order to find and quantify the influence of the strain rate on the joint response. The tests presented in this paper represent a unique set of data. In fact, despite their widespread use in some countries, the behaviour of SHJs has never been previously tested under impact loading conditions.

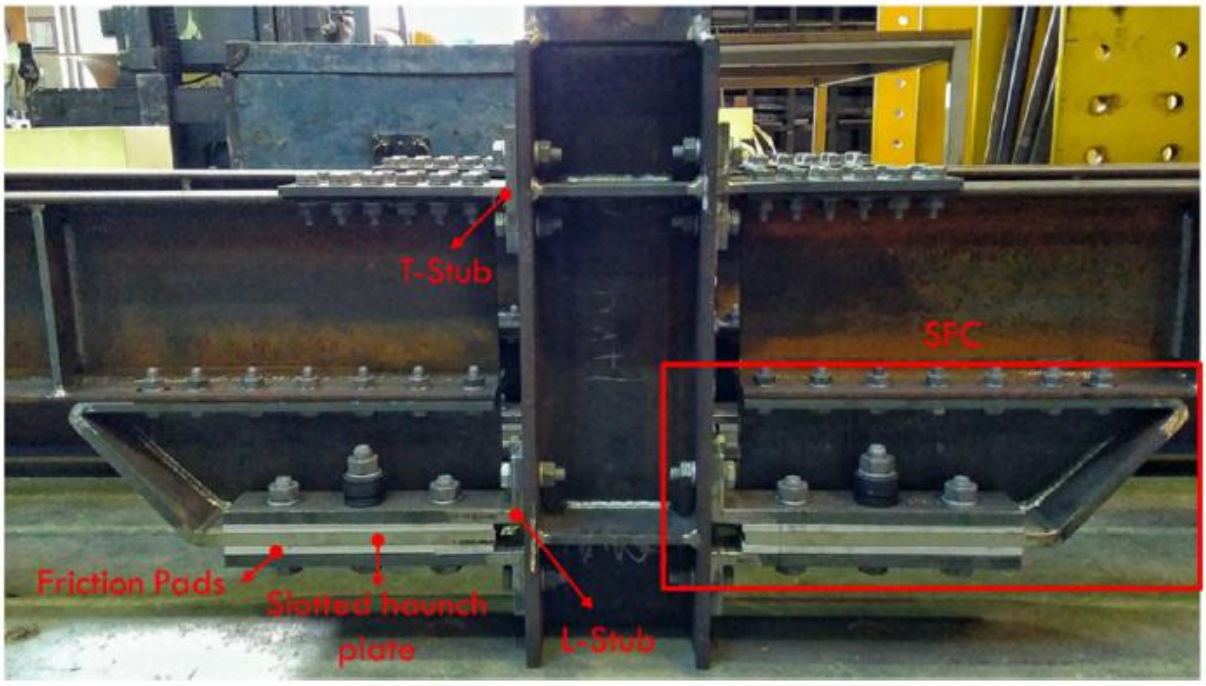

Fig. 1. SHJ joint with Symmetric Friction Damper (SFD).

2. Design of the tested SHJs

A particular SHJ configuration is tested in this work, the detailed geometry is presented in **Fig. 2**. The extended design procedure for the tested connections is detailed in [3,48,49], while the main design criteria are hereinafter briefly summarized. The tested SHJ is a modification of a Double Split Tee joint,

Published in : Journal of Constructional Steel Research (2022), vol. 192, 107215
DOI: 10.1016/j.jcsr.2022.107215
Status : Postprint (Author's version)

with a friction damper located at the bottom beam flange made of angles and pre-loaded friction shims, connected to a haunch and bolted to the lower flange of an IPE 220 beam, with preloadable M12 bolts [50], 10.9 class. To allow large rotations under bending actions, the lower plate of the haunch, which is the sliding plate of the friction damper, has slotted holes, in which the bolts are free to move up to the achievement of the slots' end. The beam upper flange is connected to the column (HE 200B) with a T-Stub and the lower flange is bolted to the haunch. Friction shims coated with specific materials are used to assure the required slip resistance and energy dissipation capacity to the joint. All the tested elements are made of S275JR steel except for the haunch sliding plate, which is made of stainless steel AISI 304. The friction damper is designed to slip under the ultimate limit state seismic event, while the non-dissipative parts of the joint are strengthened ensuring a proper dissipation only in the dissipative fuse of the connection, namely the damper.

The friction resistance of the damper can be easily designed starting from the Coulomb's friction law:

$$F_{slip} = \mu F_p n_b n_s \tag{2-1}$$

where F_p is preload in the bolts; μ is the friction coefficient; n_b is the number of the bolts and n_s is the number of friction interfaces. F_{slip} is an input design data, deriving from the structural analysis, being determined simply as the maximum design bending moment in all the ultimate limit state situations divided by the joint lever arm (h_{LA}). After that, the friction damper is geometrically defined both in terms of bolt number and in terms of design preload, all the non-dissipative parts of the connection are designed according to EC3 part 1.8 rules, adopting a proper value of the design overstrength. In the current case, since the coating material M4, previously tested in [1,10], has been adopted for the tested specimens the value of the design overstrength considered is equal to 1.9 [1,10], meaning that all the non-dissipative parts of the tested beam-to-column joints have been designed considering an increased value of the slip-resistance of the friction damper. The design value of the friction coefficient for the coating material M4 considered in the design phase is 0.53. Further details on the design of the connection are provided in [1].

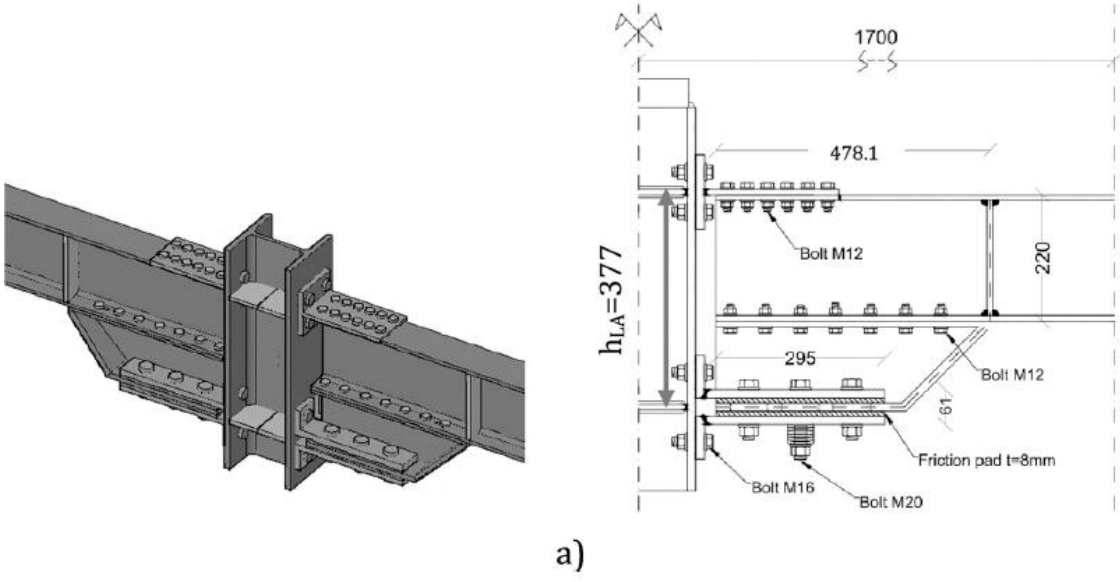

Fig. 2. a) SHJ joint; b) Lateral view; c) Joint angle; d) Haunch and pads (all dimensions are in mm).

Published in : Journal of Constructional Steel Research (2022), vol. 192, 107215
DOI: 10.1016/j.jcsr.2022.107215
Status : Postprint (Author's version)

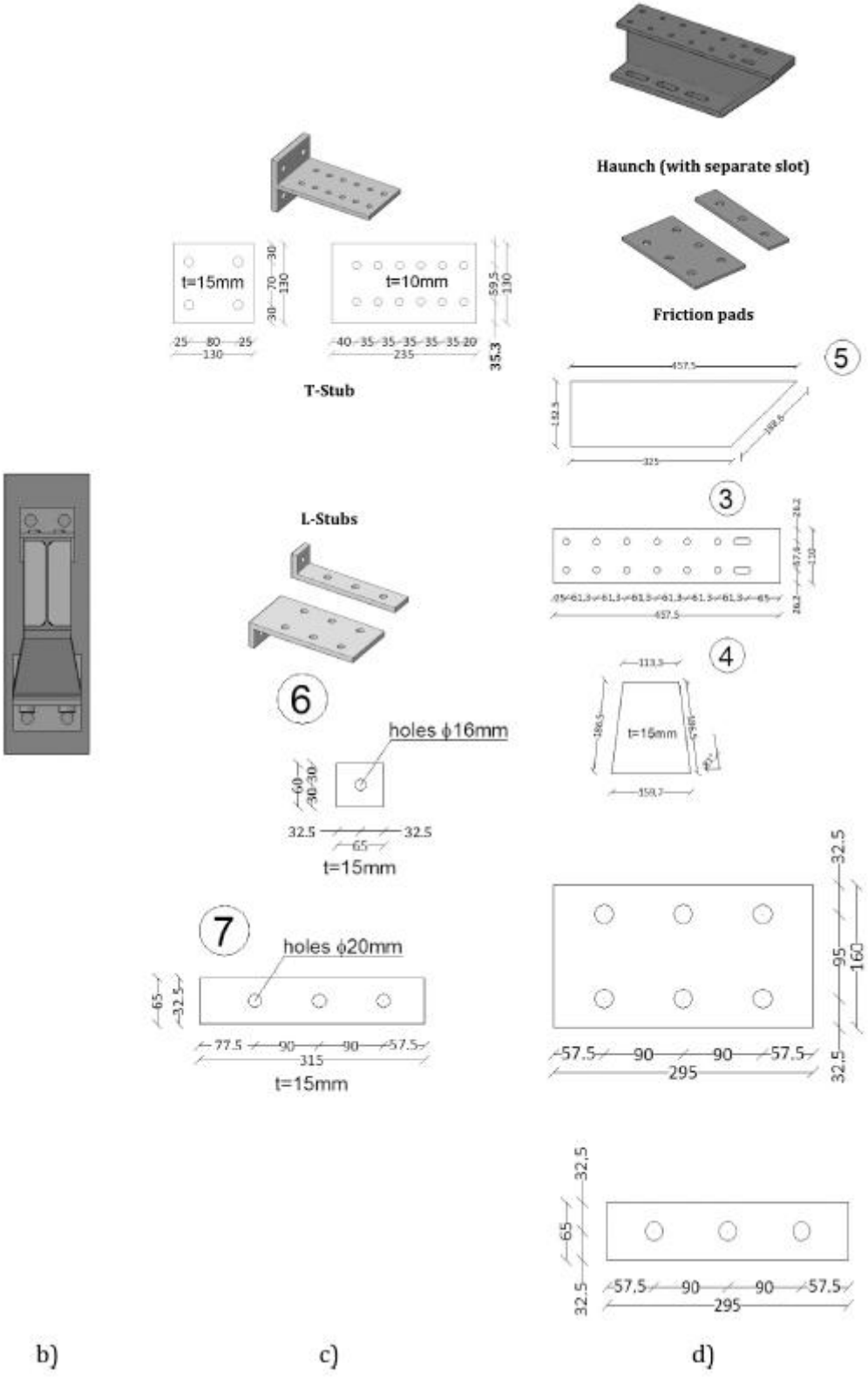

Fig. 2. *(continued)*.

Published in : Journal of Constructional Steel Research (2022), vol. 192, 107215
DOI: 10.1016/j.jcsr.2022.107215
Status : Postprint (Author's version)

3. Experimental campaign

3.1. TEST SETUP

The test campaign has included one static monotonic test and six drop-weight tests on two specimens of the same beam-to-column joint equipped with SFDs (**Fig. 3**).

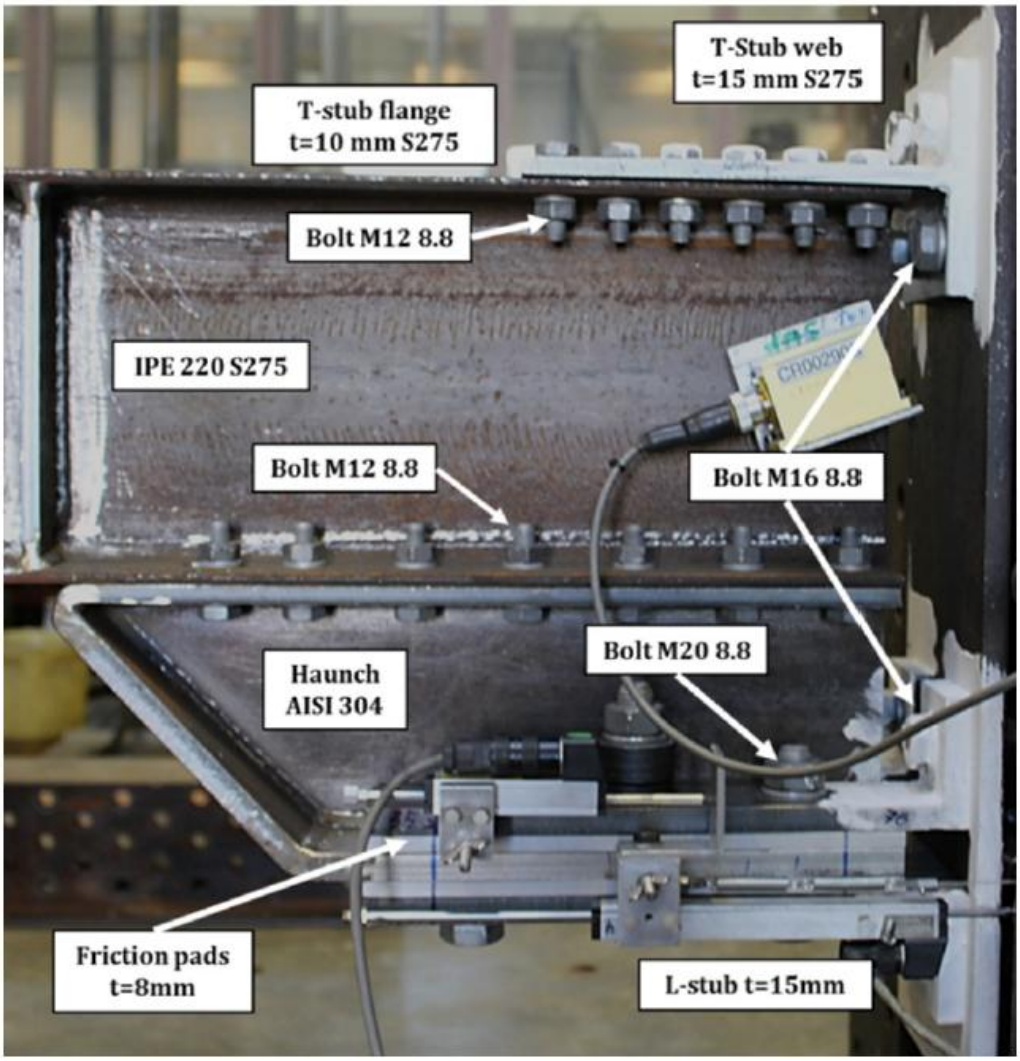

Fig. 3. Main components of the SHJ tested at the University of Liège.

The impact tests have been performed with a dropping mass, hitting the head of the column with variable speeds. Two controlling parameters are modified during the tests: the dropping mass weight and the dropping height, limited by the capacity of the instrumentation at maximum 4.1 m, calculated from the top of the impacted column. Two masses are considered in this work:211 kg (called M1) and 460 kg (called M2). These parameters are fixed according to the targeted impact energy to be reached during the tests. The dropping mass is connected to tubular guides (**Fig. 5**), which are driving the mass

Published in : Journal of Constructional Steel Research (2022), vol. 192, 107215
DOI: 10.1016/j.jcsr.2022.107215
Status : Postprint (Author's version)

until the impact and during the rebound. All the specimens are identified with an alphanumeric tag describing the main features of the test, as reported in **Fig. 4**, where the code is indicating (i) the type of test (**IT** for **I**mpact **T**est or **ST** for **S**tatic **T**est reference is made to the test presented in [49]), (ii) the joint configuration (**FR** for **FR**EEDAM joint, named after the project where the joint was developed), (iii) the number of the test (01, 02, etc.), (iv) the used mass (**M1** = 211 kg or **M2** = 460 kg) and (v) the dropping **H**eight (**H**250 means a dropping height of 250 mm).

Six impact tests and one static test (presented in detail in [1,49,51] were performed. The static test was performed for two main reasons: characterize the static behaviour of the joint and having the static equivalent force in order to estimate the DIF (see paragraph 3.3). For the impacts performed with the mass M1, the dropping heights ranged from 250 mm to 4300 mm while, for the mass M2, the heights varied from 250 mm up to 3744 mm (maximum exploitable height considering the size of the specimen and of the mass). Overall, falling speeds ranged from 2.04 m/s to 8.45 m/s. the six-impact test were performed on two specimens (in the following specimen 1 and 2) with the same geometry. Specimen 1 was subjected to five sequential impacts, while specimen 2 was impacted just one time with the maximum exploitable impact energy. A summary of the performed impact tests is provided in **Table 1**. In this table "1*", the number followed by a star stands for a sequential (or cumulative) impact on the specimen 1 (i.e. the same specimen was impacted several time).

Coupons were extracted from all the steel plates used in the production of the specimens. Static tensile tests were performed extracting samples from beams, T-stub and the L-stubs in order to define the stress- strain curves of the materials under static loading conditions. These properties are required to characterize analytically the joint and to calibrate accurately the material properties in the FE modelling. A summary of the uniaxial tensile test results is provided in **Table 2**. The presented results are average values coming from 3 tests for each element.

All the measurements during the tests were taken through Digital Image Correlation (DIC), which is an image analysis method to determine the absolute position of points, on an object surface, in two or three dimensions. Two systems were used in this experimental campaign:

- The first one, called Vision Research Phantom V710 Fast equipped with a 32 mm Zeiss lens, with a frequency of acquisition of 3 kHz, can detect the deformation of the joint and the displacement of the mass. This frequency, although it was not the maximum available, was the best compromise between the accuracy for impact and the internal storage memory capacity. This system is made of two cameras in a stereoscopic set up to register a three-dimensional movement. In other words, the cameras are looking the same object from two different positions and, knowing intrinsic and extrinsic imaging parameters through a calibration procedure, the position of a point in the space can be calculated.
- The second system of acquisition called Basler A504k (with lens Zeiss 50 mm) is composed of two independent cameras: one is used to record the mass movements and the other one as a backup for the specimens. Both are working in 2D with a frequency of 400 Hz. The 2D system is placed to ensure a backup acquisition in case of problems with the 3D one.

The two systems provided compatible and consistent results. The camera objectives (Zeiss de 32 mm and Zeiss de 50 mm) were able to cover a limited window (see **Fig. 6**); therefore, the cameras recorded

Published in : Journal of Constructional Steel Research (2022), vol. 192, 107215
DOI: 10.1016/j.jcsr.2022.107215
Status : Postprint (Author's version)

only half of the tested specimen. All the measured points are reported in the same picture. Lateral-torsional buckling was prevented during the tests using appropriate restraints.

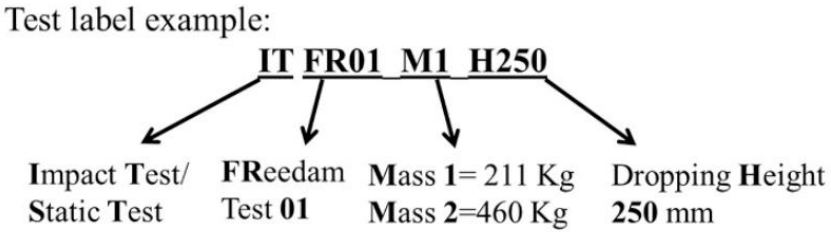

Fig. 4. Test nomenclature.

Table 1
Impact test labels and main properties of the impact.

Impact test	Specimen	M [kg]	h [m]	v [m/s]
ITFR01-M1-H250	1	211	0.25	2.04
ITFR02-M1-H4300	1*	211	4.3	8.97
ITFR03-M2-H250	1*	460	0.25	1.98
ITFR04-M2-H2000	1*	460	2	6.09
ITFR05-M2-H2500	1*	460	2.5	6.93
ITFR06-M2-H3744	2	460	3.74	8.45

Table 2
Coupon test.

Coupon	E [GPa]	$f_{0.2\%}$ [MPa]	f_u [MPa]	ε_u [%]	ε_r [%]
Beam Flange	212.9	315.2	451.5	18.0	36.7
Beam Web Test 1	212.6	343.0	475.5	31.0	42.8
T-stub web 10 mm	208.4	328,0	488.7	16.9	48.2
T-stub flange and L-stub 15 mm	202.8	372.6	529.8	13.6	43.8
AISI 304	195.4	304.7	615.6	45.5	77.8
Friction pads	207.7	392.9	515.5	17.3	40.5

Where E is Young's modulus, $f_{0,2\%}$ is the yield strength (stress for a strain equal to 0.2% indicated as $\varepsilon_{0.2\%}$, f_u is the tensile strength, ε_u and ε_r are respectively the tensile and fracture strain.

Published in : Journal of Constructional Steel Research (2022), vol. 192, 107215
DOI: 10.1016/j.jcsr.2022.107215
Status : Postprint (Author's version)

Fig. 5. Impact test layout: Mass M1 (211kg) and M2 (460 kg).

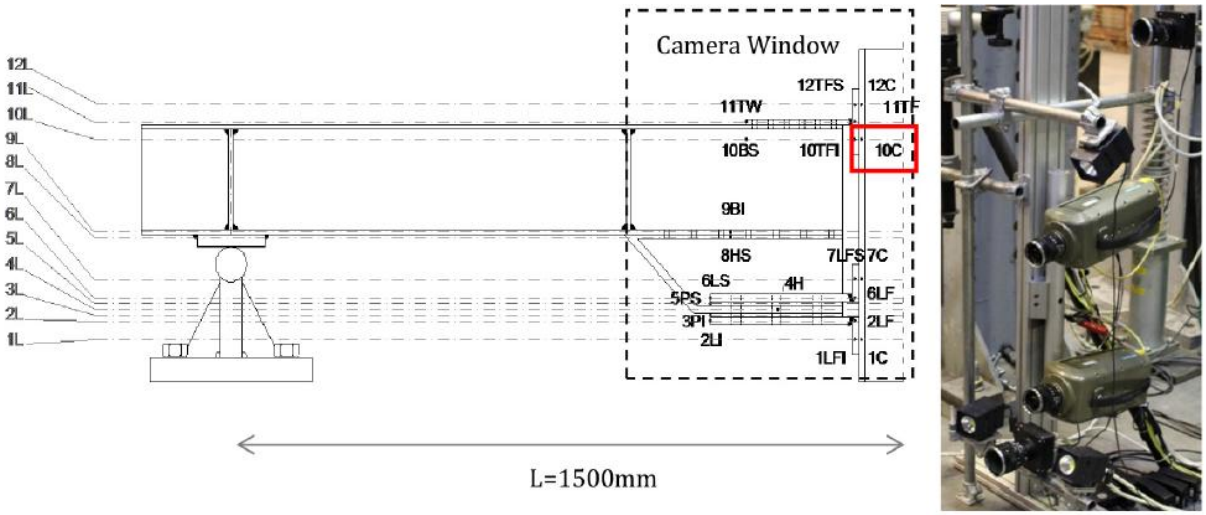

Fig. 6. Impact test configuration (half specimen), camera window (dotted line), main dimensions and identification of control point 10C.

Published in : Journal of Constructional Steel Research (2022), vol. 192, 107215
DOI: 10.1016/j.jcsr.2022.107215
Status : Postprint (Author's version)

Table 3
Impact tests results.

Impact test	h [mm]	$v_{theo,imp}$ [m/s]	$v_{act,imp}$ [m/s]	v_{reb} [m/s]	$v_{act,imp}$ / $v_{theo,imp}$	$E_{theo,imp}$ [J]	$E_{act,imp}$ [J]	COR	δ_{max} [mm]	δ_{perm} [mm]
M1 = 211 kg										
ITFR01-M1-H250	250	2.21	2.04	1.06	0.92	517.5	439.0	0.51	6.16	NA
ITFR02-M1-H4300	4300	9.18	8.97	1.49	0.98	8900.6	8488.6	0.16	56.5	46.2
M2 = 460 kg										
ITFR03-M2-H250	250	2.21	1.98	1.16	0.89	1128.2	901.7	0.58	10.2	NA
ITFR04-M2-H2000	2000	6.26	6.09	1.20	0.97	9025.2	8530.3	0.19	49.3	34.8
ITFR05-M2-H2500	2500	7.00	6.93	1.13	0.99	11,281.5	11,045.7	0.17	53.6	31.1
ITFR06-M2-H3744	3744	8.57	8.45	1.46	0.98	16,895.2	16,422.6	0.17	102.6	88.5

3.2. EXPERIMENTAL RESULTS

In this section, the impact test results are summarized, and the dynamic behaviour is evaluated. Two impact tests were performed with the mass M1 on specimen 1, namely tests ITFR01-M1-H250 and ITFR02- M1-H4300 (**Table 3**). The first test was performed with a small dropping height 250 mm remaining in the elastic domain (i.e. no plasticity was experienced by any component of the joint) while the second one, with a dropping height of 4300 mm, was performed activating plasticity in the tested specimen.

Four impact tests were performed with the mass M2: three of them (ITFR03, ITFR04 and ITFR05) on specimen 1, i.e. sequential impacts on the specimen previously tested with the mass M1, with the main objective of calibrating the testing setup with the new mass M2. The last one (ITFR06) has been performed with the maximum capacity of the system, in terms of energy and velocity, on specimen 2. However, due to the dimension of the new mass (**Fig. 5**), the maximum available dropping height was reduced from 4300 mm (max exploitable height with M1) to 3785 mm (considering the centre of gravity of the masses).

Several control points, on the main joint components, were recorded with the cameras during the tests. For some control points example are reported in **Fig. 7** where the vertical displacement vs time curves of Point 10C (see **Fig. 6**) are provided for the different impact tests. The evolutions of the displacement in time have a similar trend for all the registered points (displacement evolution). For the sake of simplicity, all the data in the following are referred to point 10C, which was chosen as a reference point, being on symmetry axis (axis of the column).

In tests ITFR01-M1-H250 and ITFR03-M2-H250, the specimens remained elastic showing negligible permanent deformations. Test ITFR02-M1-H4300 exhibited a permanent deformation of 46.2 mm at the end of the test but the level of associated plasticity in the joint components was still limited. Indeed, the energy associated to the impacts performed with mass M1 was not enough to activate plasticity in the joint components. However, the friction device exhibited a slippage of about 20 mm (**Fig. 8**) resulting in the above-mentioned permanent deformations. The bolts at the end of this test reached the end stroke of the damper.

The test with the maximum available energy and velocity (ITFR06) shown a slip of 24 mm of the damper and a vertical permanent deformation of 88.5 mm (**Fig. 9**).

Published in : Journal of Constructional Steel Research (2022), vol. 192, 107215
DOI: 10.1016/j.jcsr.2022.107215
Status : Postprint (Author's version)

In all the performed tests, theoretical velocities calculated for the impact ($v_{theo,imp}$ – see Eq. (3-1)) are slightly different from the one detected by the acquisition system ($v_{act,imp}$). Indeed, the real velocities are usually lower than the theoretical ones and, accordingly, the same is observed for the energies ($E_{act,\ imp}$ is the actual Energy and $E_{theo,\ imp}$ the theoretical one – see Eq. (3-2)) defined through the following equations:

$$v_{theo,imp} = \sqrt{2gh} > v_{act,imp} \tag{3-1}$$

$$E_{theo,imp} = \frac{1}{2}mv_{theo,imp}^2 > E_{act,imp} \tag{3-2}$$

where *g* is the gravitational acceleration, *m* is the weight of the dropped mass and *h* is the dropping height. In **Table 3**, actual and theoretical values of impact velocities and energies are compared, showing that the lower is the dropping height, the higher is the scatter. The observed difference is mainly associated with the friction developing between the dropping mass and the guiding system which is not considered in the theoretical estimation. However, in all the tests, the ratio between the actual velocity and the real one is close to 1, showing a small influence of the testing rig on the development of the expected impact velocity. In the same table, the values of the maximum (δ_{max}) and permanent (δ_{perm}) deflections of the joint at the point 10C (see **Fig. 6**) are also reported. For the sequential impact (ITFR03, ITFR04 and ITFR05), the permanent displacement is referring to the previous test, the *i-th* maximum displacement ($\delta_{max,i}$) should be summed to the permanent displacements of all the previous impacts. Generally speaking, an increase of the dropping height results in an increase of the permanent deformation magnitudes.

If the impact velocity is close to the rebound speed, namely the velocity when the impactor leaves the body, the impact is considered elastic. In reality, an impact is never completely elastic, part of the energy being used to deform the impacted body. The nature of the impact can be characterized by the ratio of these velocities called Coefficient of Restitution "*COR*" (see Eq. (3-3)), given in **Table 3**. A value of this COR close to one means that the response of the specimen is mainly elastic.

$$COR = \frac{v_{reb}}{v_{theo,imp}} \leq 1 \tag{3-3}$$

The COR is varying from 0.58 for ITFR03 to 0.16 for ITFR02. The latter shows that increasing the energy of impact (mass weight and/or height) leads to more dissipation of energy through the activation of plastic deformations; thus, the impact becomes strongly inelastic.

In **Fig. 10**, raw images captured by the 3D cameras system are reported, at different levels of displacement, for the test ITFR06-M2–3744.

From this raw registration, the selected points are tracked, and the displacements are identified. In the pictures, the green box is representing the impactor and the yellow dotted line is the reference initial position of the joint.

As the impact takes place (at *t* = 0.007 s) the joint starts to rotate (the initial position of the damper is represented by yellow dotted line) until reaching the maximum vertical displacement of the system

Published in : Journal of Constructional Steel Research (2022), vol. 192, 107215
DOI: 10.1016/j.jcsr.2022.107215
Status : Postprint (Author's version)

(mass + joint, t = 0.036 s). After this point the mass rebounds and begins to move upwards. Afterwards the mass hits the specimen several times before stopping.

At the end of the impact tests, the achievement of a considerable level of plasticity in the L-stubs and the T-stubs of the joints was detected (**Fig. 11** a and c). Additionally, also the slippage of the friction device and the consumption of the pads coating materials were visible (**Fig. 11** b and d).

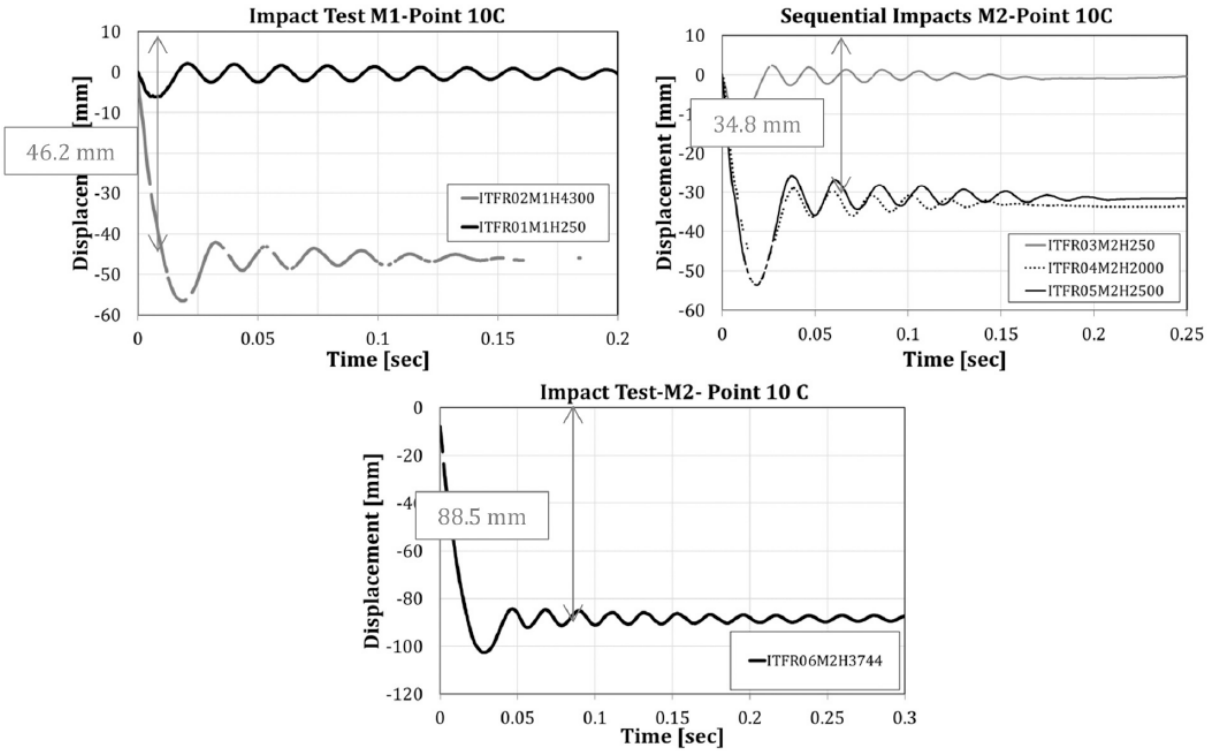

Fig. 7. Impact test results – examples of point displacement vs. time measurements for the point 10C.

Fig. 8. Impact test results ITFR 02 M1 H4300 – slippage of the friction device.

Published in : Journal of Constructional Steel Research (2022), vol. 192, 107215
DOI: 10.1016/j.jcsr.2022.107215
Status : Postprint (Author's version)

Fig. 9. Impact test results ITFR 06 M2 H3785 – slippage of the friction device.

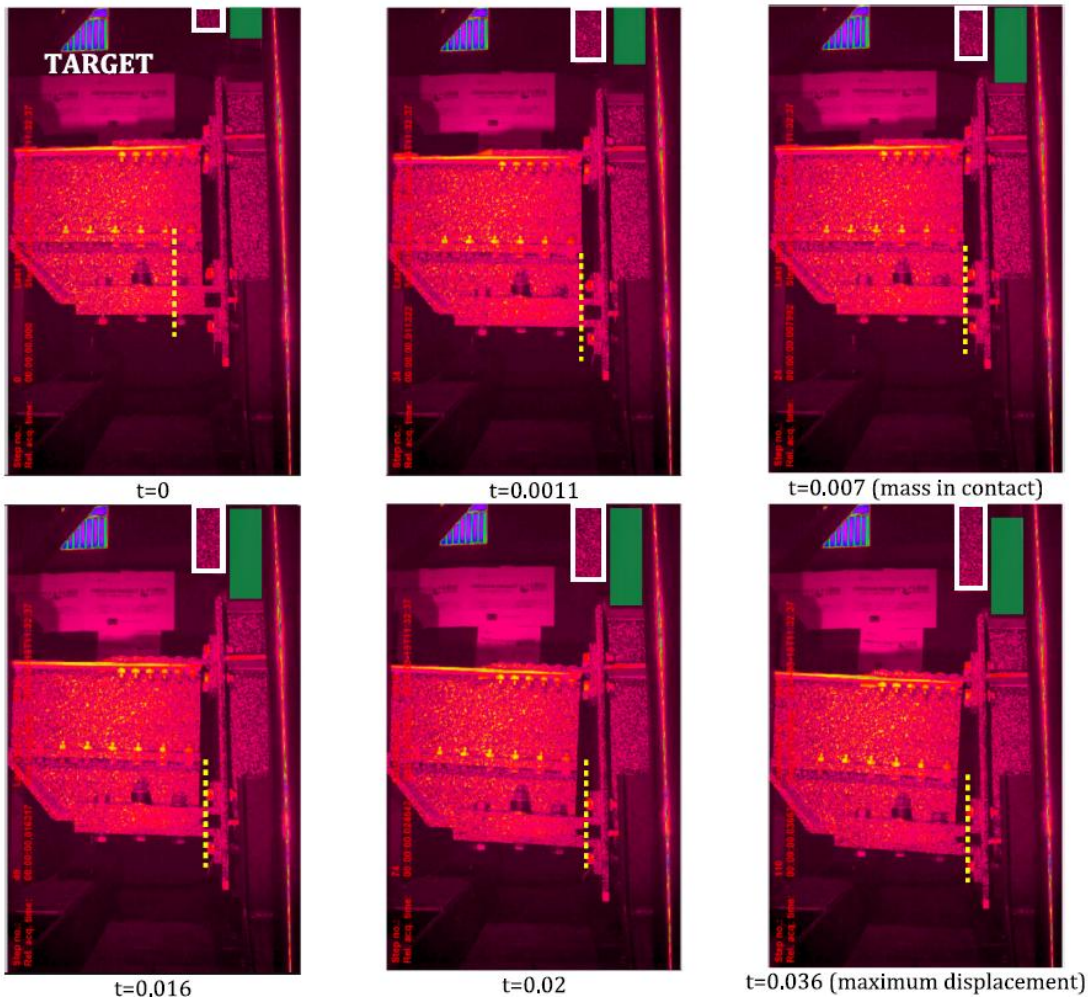

Fig. 10. Images captured with 3d camera system.

Published in : Journal of Constructional Steel Research (2022), vol. 192, 107215
DOI: 10.1016/j.jcsr.2022.107215
Status : Postprint (Author's version)

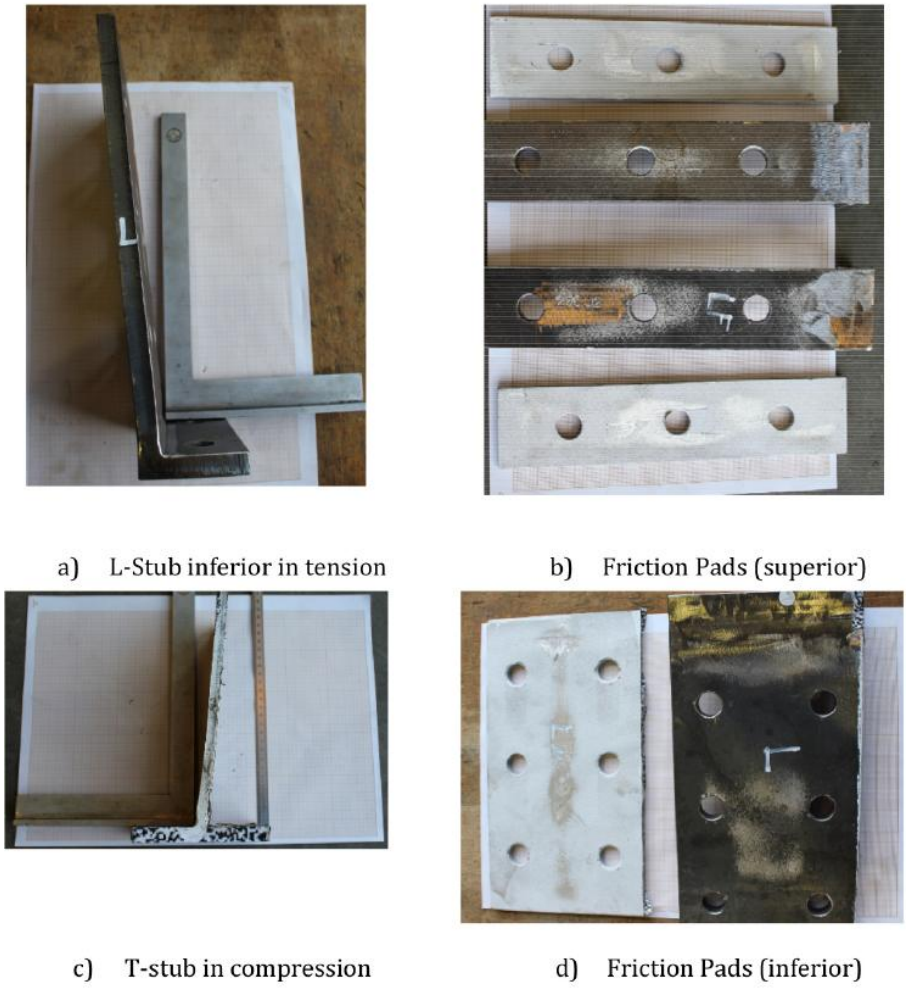

Fig. 11. Impact test results – deformation of the angles (a-c) and consumption of the friction plates (b-d).

3.3. IMPACT FORCE ESTIMATION

Due to the limitations in the laboratory facilities, the impact force was not directly registered during the tests. Two estimation methodologies were adopted to measure the forces indirectly: the impulse-momentum theorem and a graphic approach, following the same procedure presented in [1,47]. A first estimate of the impacting force has been done through the impulse-moment theorem, which allows to assess indirectly the impact force F_{IT} through Eq. (3-4), starting from the measurement of the pulse width (t_{pulse} measured with the DIC system).

$$\overrightarrow{F_{IT}}\,\Delta t = m\Delta\vec{v} \rightarrow \overrightarrow{F_{IT}} = m \cdot \frac{\vec{v}_{act,imp} - \vec{v}_{reb}}{t_{pulse}} \tag{3-4}$$

with the graphic method, the force associated to each impact is estimated starting from the knowledge of the static response of the joint, the maximum deformation (δ_{max}) experienced during the impact, the permanent deformation (δ_{perm}) and the initial stiffness of the joint ($S_{j,ini}$). The graphical construction

Published in : Journal of Constructional Steel Research (2022), vol. 192, 107215
DOI: 10.1016/j.jcsr.2022.107215
Status : Postprint (Author's version)

adopted is described in **Fig. 12**. In the same figure, also the equivalent static resistance (F_{ST}) associated with each test is indicated.

Table 4 gives a summary of the application of the two methodologies for the maximum impact force estimation. Even though the two methodologies are indirect measures, they show a similar estimate of the impacting force, which is reported in **Table 4**.

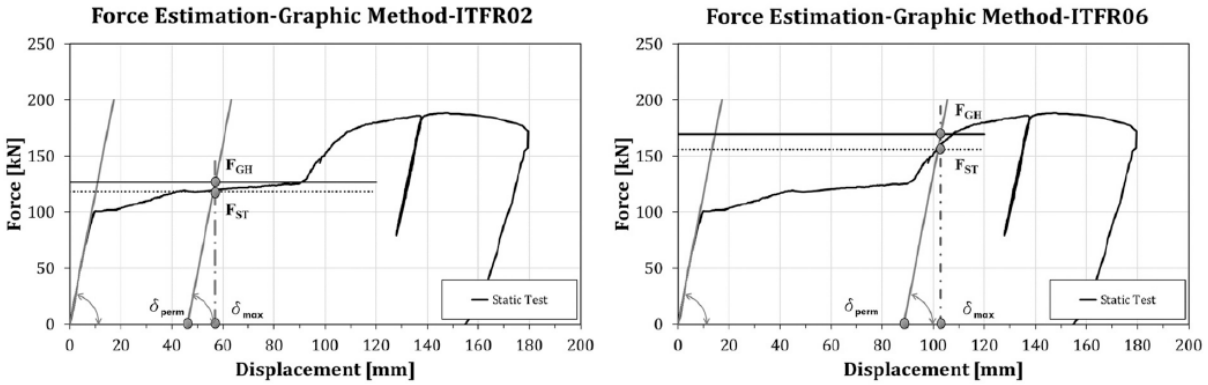

Fig. 12. Graphic estimation of the DIF.

4. FEM modelling

4.1. MODEL DESCRIPTION

To extend the results beyond the range of geometries examined in the experimental work, a finite element model reproducing the specimen behaviour under impact was developed using ABAQUS/CAE [49,52,53] (explicit time integration). Two analysis methods are available in Abaqus to solve structural problems, namely Abaqus/Standard and Abaqus/Explicit. Abaqus/Standard has both static implicit and dynamic implicit analyses, the difference is not in the physic event (static or dynamic) but in the analysis methods used to solve problems. To discretize the equation of motion, the implicit analysis method uses backwards Euler time integration, which is numerical methods to solve ordinary and partial differential equations. The solution at a given time step depends on the state of the system at the previous step. On the contrary in explicit methods (used for impact) the state of a system at a given time step from the state of the system at the current time step.

The model replicates the tested geometry in a 3D environment. In particular the model replicates half of the subassembly tested in the experimental campaign. The extremity of the beam is supported by a vertical roller; hence, the axial translation is unrestrained. Additionally, the numerical model was developed taking advantage of symmetry, considering only half specimen, introducing symmetry constraints in the middle of the column (**Fig. 13**a).

The impact has been reproduced modelling a 3D discrete rigid body with isotropic inertia meshed using rigid elements. Tie constraints were used to connect the stiffeners to the beam and the column. A

Published in : Journal of Constructional Steel Research (2022), vol. 192, 107215
DOI: 10.1016/j.jcsr.2022.107215
Status : Postprint (Author's version)

general contact was introduced for all the elements, with a "hard contact" definition in the normal direction and a tangential behaviour with a friction coefficient equal to 0.3. The key element, the friction shims have a friction coefficient of 0.53. The contact between the friction pads and the slotted haunch plate was defined with a surface-to-surface contact, with specific tangential friction (detailed in [1]) and a normal behaviour following the classical Coulomb friction model.

The modelled hammer was placed initially directly in contact with the tested specimen, assigning to the mass the value of the impacting velocities measured during the tests ($v_{act,imp}$ given in **Table 4**). The model sensitivity to the element type was initially analysed, comparing the accuracy of the results with two different finite element types, namely the C3D8R with enhanced hourglass control and the C3D8. The first is a linear brick element with reduced integration (1 integration point) while C3D8 has eight integration points. Despite the efficient hourglass control available in the software, C3D8 full integration was selected as the most appropriate one. Hourglass problems can appear when reduced integration is used, to avoid this, the artificial strain energy of the model (ALLAE in ABAQUS) should be small enough (less than 5%) when compared to the Internal energy (ALLIE) [54], which was the case for the presented simulations (**Fig. 13**b).

A mesh sensitivity study was also performed in order to select the best mesh compromise between the accuracy of the results and analysis time. The best compromise was obtained with a mesh composed of 33,737 elements for a total analysis time in between 20 and 48 h for each simulation, depending also on the output requests. The optimized mesh considered for the FE modelling was variable with a refinement in zone where higher plastic deformation were expected.

The bolts are modelled using the nominal diameter and scaling the material nominal stress as explained in [6,44,45,55,56]. The bolt preload is applied to the middle section of the bolt shank, using the option "Bolt Force". Following the procedure given in [47,57] the damping was modelled with the classical Rayleigh theory calibrating only the mass proportional coefficient (a). The calibration of the damping was done calculating the first natural frequency of vibration of the system equal to 324 rad/s and the damping ratio using the elastic impacts ITFR01 and ITFR03. The mass proportional coefficient was equal to a = 11 corresponding to a damping ratio of approximately 2% (**Fig. 14**). The analysis was performed in two steps: in a first step, the bolts were preloaded and, subsequently, in a second step the dynamic load was applied.

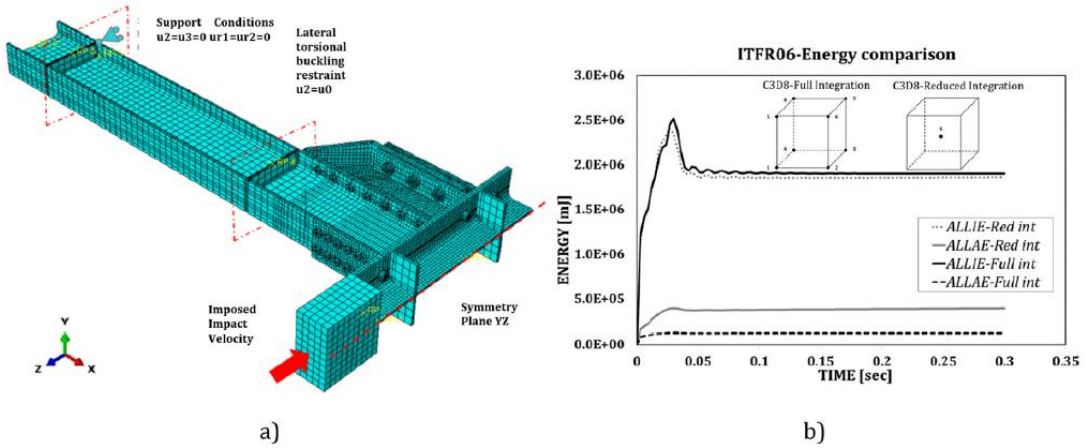

a) b)

Fig. 13. FEM detail and energy comparison.

Published in : Journal of Constructional Steel Research (2022), vol. 192, 107215
DOI: 10.1016/j.jcsr.2022.107215
Status : Postprint (Author's version)

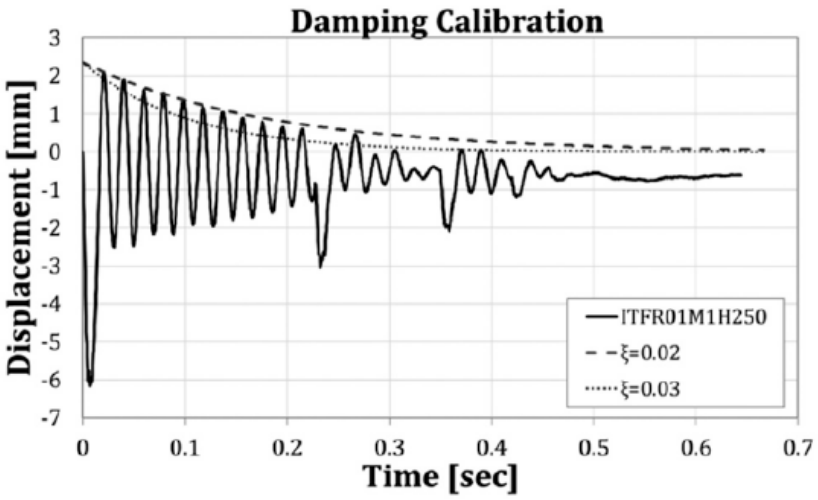

Fig. 14. Damping calibration.

Table 4
DIF calculation.

Test	δ_{max} [mm]	δ_{perm} [mm]	$v_{act,imp}$ [m/s]	v_{reb} [m/s]	t_{pulse} [s]	F_{ST} [kN]	F_{GR} [kN]	F_{IT} [kN]	DIF_{GR}	DIF_{IT}
Mass M1 ITFR02 M1 H4300	56.5	46.2	8.97	1.49	0.018	118.5	123.1	122.6	1.039	1.03
Mass M2 ITFR06 M2 H3744	102.6	88.5	8.45	1.46	0.027	158.7	164.6	168.8	1.037	1.06

*Where *M* is the dropping mass; $v_{act,imp}$ is the measured velocity; v_{reb} is the measured velocity of the first bounce; t_{pulse} is the impact width pulse, F_{ST} is the equivalent static force, F_{GR} is the impact force estimated with the graphic method and F_{IT} are the maximum impact force evaluated with the impulse theorem.

4.1.1. MATERIAL BEHAVIOUR AND DAMAGE MODEL AND STRAIN RATE

The material models implemented in Abaqus were calibrated on the available coupon tests. The engineering curves were implemented in ABAQUS as true stress true strains curves with a Young modulus of 210 GPa and a Poisson's ratio of 0.3. Ductile damage material is implemented following the procedure given by Pavlović in [43]. The hardening part of the curve is described by the undamaged material response. To describe the evolution of the softening part of the material behaviour curve, damage initiation and damage evolution criteria need to be defined. The damage initiation needs the definition of the equivalent strain at the onset of damage $\overline{\varepsilon_0^{pl}}$ (D = 1 in **Fig. 15**) as a function of the stress triaxiality and true plastic strain at the necking point ε_n^{pl}.

$$\overline{\varepsilon}_0^{pl}(\eta) = \varepsilon_n^{pl} \cdot e^{-1.5(\eta-1/3)} \quad (4\text{-}1)$$

The damage was introduced only in the parts in which high plasticity was expected: T-Stub, L-stubs and bolts. Damage evolution was defined starting from the experimental tests, using a reverse approach and calibrating the parameters by modelling the coupons tests in Abaqus (**Fig. 15**). The required parameters for this process are: the displacement at failure $\overline{u_f^{pl}}$, the plastic strain at necking ε_n^{pl}, the fracture strain ε_f^{pl} (both taken from the experimental curves) and the size of the finite element L_E. In

Published in : Journal of Constructional Steel Research (2022), vol. 192, 107215
DOI: 10.1016/j.jcsr.2022.107215
Status : Postprint (Author's version)

the ABAQUS software, $\overline{u_f^{pl}}$ can be introduced with a linear evolution (Eq. (4-3)). The latter approach has been used except for the bolts for which no test results were available as explained hereafter.

$$\overline{u}_f^{pl} = \left(\varepsilon_f^{pl} - \varepsilon_n^{pl}\right) \cdot L_E \tag{4-2}$$

$$\overline{u}_i^{pl} = \overline{u}_f^{pl} \cdot \left(\frac{\varepsilon_i^{pl} - \varepsilon_n^{pl}}{\varepsilon_f^{pl} - \varepsilon_n^{pl}}\right) \tag{4-3}$$

Bolt modelling is implemented following the simplified model with an equivalent shank suggested in [45]. The approach consists in using the gross nominal area of the bolt and to account for the threads with a reduced Young's modulus (130 GPa), while the plastic behaviour is modelled scaling down the experimental curve to fictitiously simulate the bolt behaviour. Since no coupon tests were performed on the bolts used for the tests, reference is made to the tests reported in [44].

The ductile damage parameters were also taken from the previous study on the same type of bolts [3,45] and are reported in **Table 5**.

For dynamic loadings, the strain rate needs to be implemented in the model. Johnson-Cook model was adopted (Eq. (4-4)) with the parameters reported in **Table 6**.

$$\frac{\sigma_{dyn}}{\sigma_{stat}} = DIF = \left(1 + C ln \frac{\dot{\varepsilon}_p}{\dot{\varepsilon}_0}\right) \tag{4-4}$$

The value of C for S275 steel has been calibrated by the same authors in a former test campaign presented in [47]. The value of *C* for the AISI 304 and the bolts are coming from the literature [26,58]. In **Table 6**, the value of C_u, which is referring to a DIF related to the increase of ultimate resistance, is also introduced. This value will be used in the next section in order to identify the influence of strain rate on the joint failure. Also the values of C_u reported in **Table 6** are taken from the literature [59].

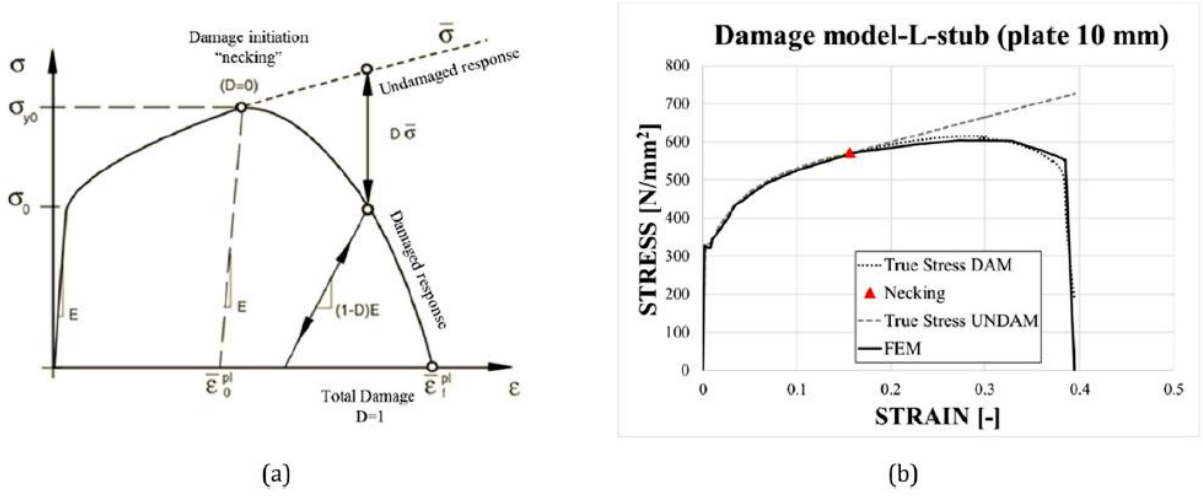

Fig. 15. Calibration of damage: (a) Abaqus model; (b) Model calibration on real tests.

Published in : Journal of Constructional Steel Research (2022), vol. 192, 107215
DOI: 10.1016/j.jcsr.2022.107215
Status : Postprint (Author's version)

Table 5
Damage calibrated values.

DAMAGE MODEL	ε_n^{pl}	ε_f^{pl}	$\overline{u_f^{pl}}$	L_E [mm]
Steel 275 Plate 10 mm	0.15	0.39	0.33	1.4
Steel 275 Plate 15 mm	0.12	0.36	0.32	1.4
Bolts 10.9	0.15	NA	0.1	5

Table 6
Parameter.

Material	$\dot{\varepsilon_0}$ [s^{-1}]	C	C_u
Steel 275	0.001	0.039	0.039
Stainless steel	0.001	0.03	0.0093
Bolts 10.9	0.001	0.0072	0.0047

4.2. VALIDATION

4.2.1. MODEL VALIDATION

In **Fig. 16**, the displacement of the reference point (10C-**Fig. 6**) predicted by the FEM, has been compared with the experimental tests (dotted line). The comparisons show a good agreement between the experiments and the FEM.

In **Table 7**, the comparison between the experimental results and the FEM analyses is reported in terms of maximum and permanent displacement (δ_{max} and δ_{perm}) with the relative errors in the prediction. Overall, the FEM seems to predict with good accuracy the two values with a maximum error of around 9% for the test ITFR01.

Besides, for the test ITFR02-M1-H4300, a comparison between the FEM results and the experiments in term of plastic damage distribution (PEEQ, cumulative plastic deformation) at the end of the test is delivered in **Fig. 17**. The distribution of cumulative plastic deformations in the FE and the experiment show a similar distribution mainly concentrated in the angles. The final stage in terms of permanent deformation and stress distribution at the end of the test is also represented in **Fig. 18** comparing the FE results with the experiments.

The FEM model was used to estimate the impact force summing the reactions at the support points. The evolution of force in time is given in **Fig. 19** for two tests (ITFR02M1H4300 and ITFR06M2H3744). To clean the signal, a zero-phase digital filtering procedure is used, the same procedure given in [47] is here used.

For the calculation of the DIF, the ratio between the dynamic and static resistance was calculated. **Table 8** gives a comparison between the DIFs calculated with different methods. From the comparison, it seems that the impulse theorem underestimates the DIF values.

Published in : Journal of Constructional Steel Research (2022), vol. 192, 107215
DOI: 10.1016/j.jcsr.2022.107215
Status : Postprint (Author's version)

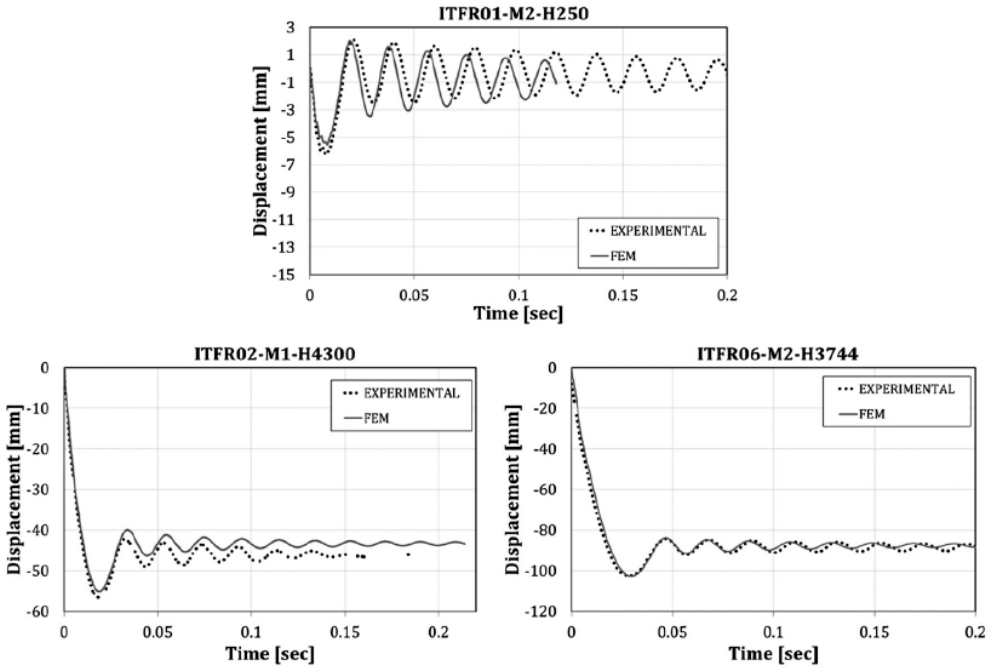

Fig. 16. Experimental tests vs FE modelling.

Table 7

Comparison of FEM experimental

Impact test	$\delta_{max,Exp}$ [mm]	$\delta_{perm,Exp}$ [mm]	$\delta_{max,FEM}$ [mm]	$\delta_{perm,FEM}$ [mm]	$\%_{err,\delta max}$ [–]	$\%_{err,\delta per}$ [–]
ITFR01-M1-H250	6.16	–	5.6	–	9.09%	–
ITFR02-M1-H4300	56.7	46.2	55.1	43.9	2.82%	4.98%
ITFR06-M2-H3744	102.6	88.5	102.8	87.8	0.19%	0.79%

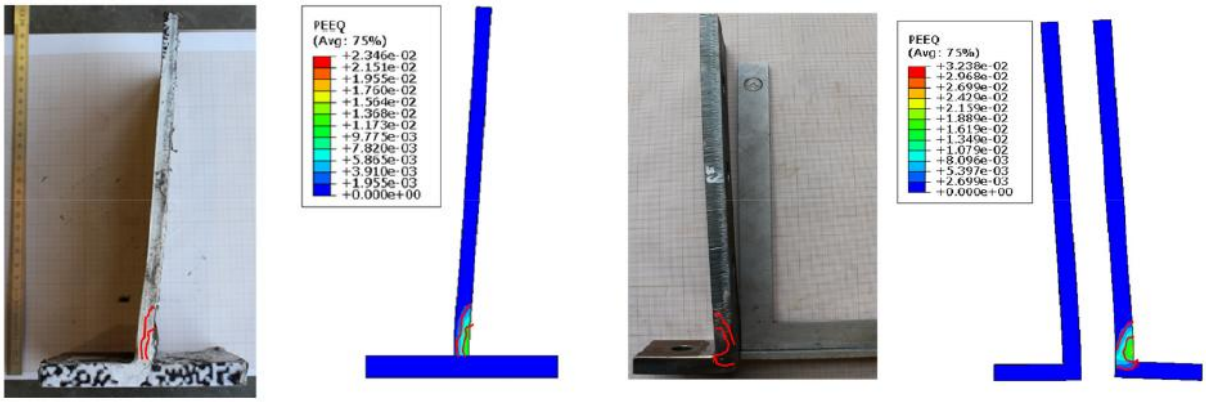

Fig. 17. Plastic damage distribution (PEEQ, cumulative plastic deformation) at the end of the test ITFR02-M1-H4300.

Published in : Journal of Constructional Steel Research (2022), vol. 192, 107215
DOI: 10.1016/j.jcsr.2022.107215
Status : Postprint (Author's version)

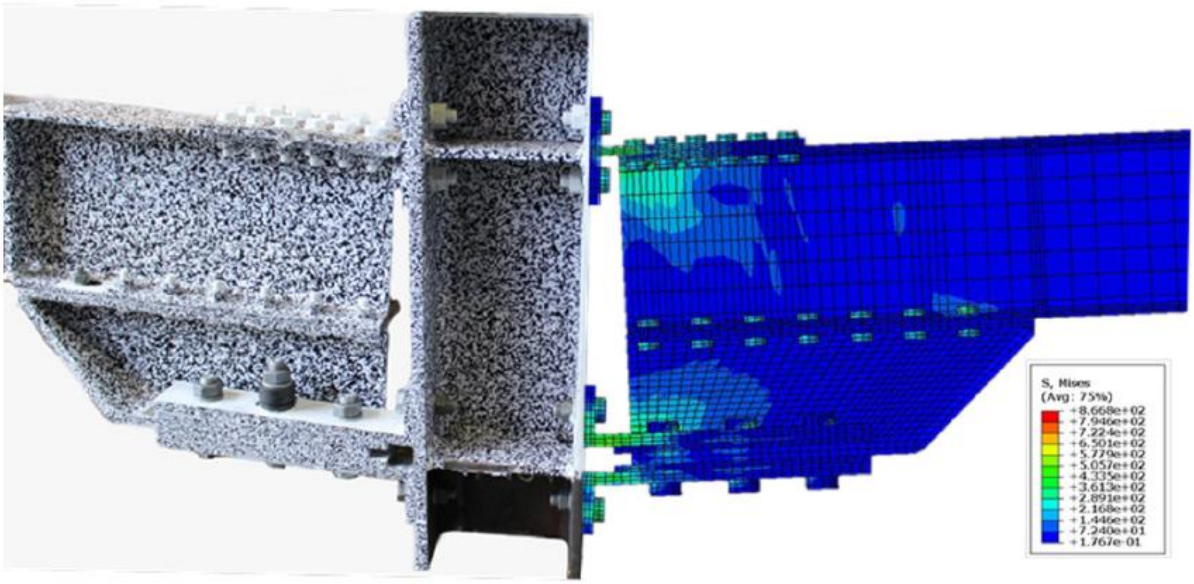

Fig. 18. Tested specimens and stress distribution (S, Von Mises criterion) in the FE analysis at the end of the test ITFR02-M1-H4300.

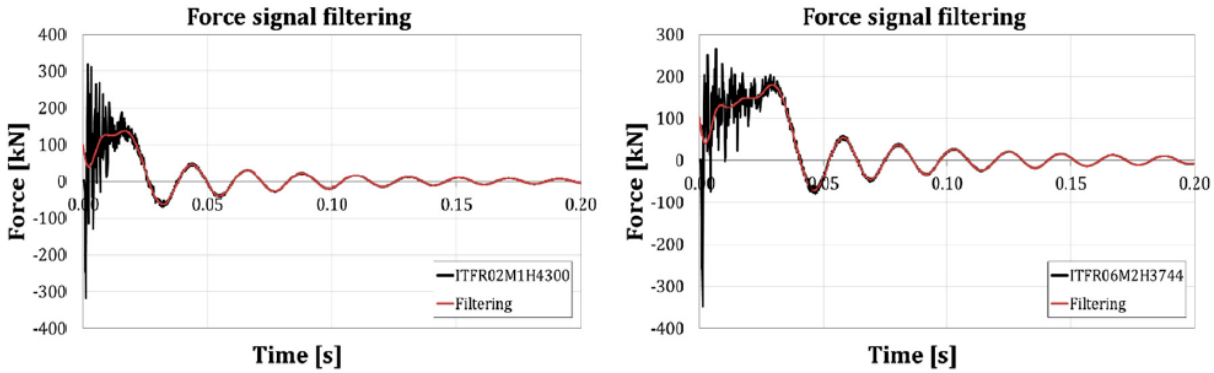

Fig. 19. Signal filtering to obtain the evolution the impact force.

4.3. PARAMETRIC ANALYSIS

With the help of the validated FE model, parametric analyses have been performed to extend the experimental results. Overall, the most important parameter influencing the joint behaviour is the impact energy as stated also in other works [], but different joint behaviours can be identified when different impact masses or velocity are used.

In this part of the work, the effect of the energy on the overall behaviour is investigated through the variation of three parameters: Mass, Velocity and energy. In particular, from the parametric study, the energy dissipation capacity of the joint, which is the best parameter to classify its response, is characterized through the Energy dissipation rate [36].

More in details, three groups of parametric analyses were performed:

- The first group (**Group 1**) investigates the influence of the impact velocity with three different mass weights (constant).

Published in : Journal of Constructional Steel Research (2022), vol. 192, 107215
DOI: 10.1016/j.jcsr.2022.107215
Status : Postprint (Author's version)

- **Group 2** investigates the influence of the mass weight variation on the joint response keeping constant the velocity.
- The last group (**Group 3**) investigates the influence of the contemporary variation of mass and velocity keeping constant the impact energy.

A summary of the examined cases is given in **Table 10** for each of the group of analyses. The name of each parametric test is an alphanumeric string where the first two letters are for "Parametric Test" (PT), the second part is indicating the Mass weight (from M1 to M9 – see **Table 9**) after there is an indication of the impact Velocity (V1-V10 – see **Table 9**) and the last part of the name is indicating the impact Energy (E1 to E10 – see **Table 9**). Energy dissipation rates, dynamic increase factors, peak displacement and internal forces are compared in each simulation. Different behaviour can be recognized according to the varied parameter as detailed in the following sections.

The values of *M* and *E*, given in **Table 10** and listed in **Table 9**, are referring to half of the model (half of the energy of the model is called E* in **Table 10**). However, in reality, due to the symmetry of the system, the masses and the energies are doubled (e.g. it means that M1 is 0.106 in the FEM model but, due to the symmetry, the total mass is 0.211 ton).

Table 9
Tested values of M, V and E.

Masses "M" [ton] (On half specimen)		*Velocities "V"* [m/s]		*Energies "E"* [mJ]	
M1	0.106	V1	8.57	E1	8.45E+06
M2	0.23	V2	9.90	E2	1.13E+07
M3	0.3	V3	12.53	E3	1.81E+07
M4	0.35	V4	14.01	E4	2.26E+07
M5	0.4	V5	6.26	E5	5.89E+06
M6	0.45	V6	8.76	E6	1.08E+07
M7	0.5	V7	7.67	E7	1.47E+07
M8	0.55	V8	7.10	E8	2.35E+07
		V9	5.94	E9	4.51E+06
		V10	5.67	E10	7.85E+06
				E11	8.83E+06
				E12	9.81E+06
				E13	3.89E+06
				E14	5.20E+06

Published in : Journal of Constructional Steel Research (2022), vol. 192, 107215
DOI: 10.1016/j.jcsr.2022.107215
Status : Postprint (Author's version)

Table 10
Parametric tests.

		Test number	Test code	Mass [ton]	v [m/s]	E* [mJ]	FAILURE (B=BOLT)
GROUP 1	M2 = Constant =0.23 t V = variable	1.1	PT-M2-V1-E1	0.23	8.57	8.45E+06	NO
		1.2	PT-M2-V2-E2	0.23	9.90	1.12E+07	NO
		1.3	**PT-M2-V3-E3**	**0.23**	**12.53**	**1.80E+07**	**FAILURE-B**
		1.4	**PT-M2-V4-E4**	**0.23**	**14.01**	**2.25E+07**	**FAILURE-B**
	M3 = Constant =0.3 t V = variable	1.5/2.2	PT-M3-V5-E5	0.3	6.26	5.87E+06	NO
		1.6	**PT-M3-V1-E6**	**0.3**	**8.57**	**1.10E+07**	**FAILURE-B**
		1.7	**PT-M3-V2-E7**	**0.3**	**9.90**	**1.47E+07**	**FAILURE-B**
		1.8	**PT-M3-V3-E8**	**0.3**	**12.53**	**2.35E+07**	**FAILURE-B**
	M1 = Constant =0.106 t V = variable	1.9	PT-M1-V1-E13	0.106	8.57	3.89E+06	NO
		1.10	PT-M1-V2-E14	0.106	9.90	5.20E+06	NO
		1.11	PT-M1-V3-E1	0.106	12.53	8.32E+06	NO
		1.12	PT-M1-V4-E6	0.106	14.01	1.10E+07	NO
GROUP 2	V5 = Constant = 6.26 m/s M = variable	2.1	PT-M2-V5-E9	0.23	6.26	4.51E+06	NO
		2.2/1.5	PT-M3-V5-E5	0.3	6.26	5.87E+06	NO
		2.3	PT-M4-V5-E9	0.35	6.26	6.87E+06	NO
		2.4	PT-M5-V5-E10	0.4	6.26	7.85E+06	NO
		2.5	PT-M6-V5-E11	0.45	6.26	8.83E+06	NO
		2.6	PT-M7-V5-E12	0.5	6.26	9.81E+06	NO
		2.7	**PT-M8-V5-E6**	**0.55**	**6.26**	**1.10E+07**	**FAILURE-B**
GROUP 3	E11 = Constant = 8.83E+06 mJ M, v = variable	3.1	PT-M2-V6-E11	0.23	8.76	8.83E+06	NO
		3.2	PT-M3-V7-E11	0.3	7.67	8.83E+06	NO
		3.3	PT-M4-V8-E11	0.35	7.10	8.83E+06	NO
		3.4/2.5	PT-M5-V5-E11	0.45	6.26	8.83E+06	NO
		3.5	PT-M7-V9-E11	0.5	5.94	8.83E+06	NO
		3.6	PT-M8-V10-E11	0.55	5.67	8.83E+06	NO

5. Results of the parametric analysis

5.1. EFFECT OF THE VARIATION OF THE IMPACT VELOCITY (V)

The first investigated parameter influencing the joint behaviour is the impact velocity (v). Different velocities were investigated with the three considered masses (see **Table 10**, Group 1). In group 1, for Mass 1, Mass 2 and M3 were kept constant while v was variating until reaching the failure of the connection. The results in terms of displacement vs time and force vs displacement are given in **Fig. 20**; in particular, graphs b) to d) provide a comparison with the static behaviour. From the comparison between the maximum impact force in Group 2 and the static behaviour of the connection, the increase of resistance for the same level of displacement (d_{max} in the impact tests) is highlighted. The highest impact velocity with the mass M2 = 0.23 t is equal to 9.90 m/s. With the mass M3, only one impact was performed with a velocity of 6.26 m/s. Indeed, a further increase of velocity in both cases always brings to the failure of the bolts of the lower L-stub. Higher impact velocity corresponds to higher maximum and permanent deformations. Moreover, *v* influences significantly the impact forces: even a small variation of *v* brings a high variation of impact forces, as it can be seen in the following **Table 11**.

In **Fig. 20** b), c) and d) the comparison with the static behaviour shows how the dynamic effect influences the response of the SHJ. Comparing the dynamic force with the equivalent static force, estimated at the same level of displacement, gives a magnitude of the DIF for each simulation.

Published in : Journal of Constructional Steel Research (2022), vol. 192, 107215
DOI: 10.1016/j.jcsr.2022.107215
Status : Postprint (Author's version)

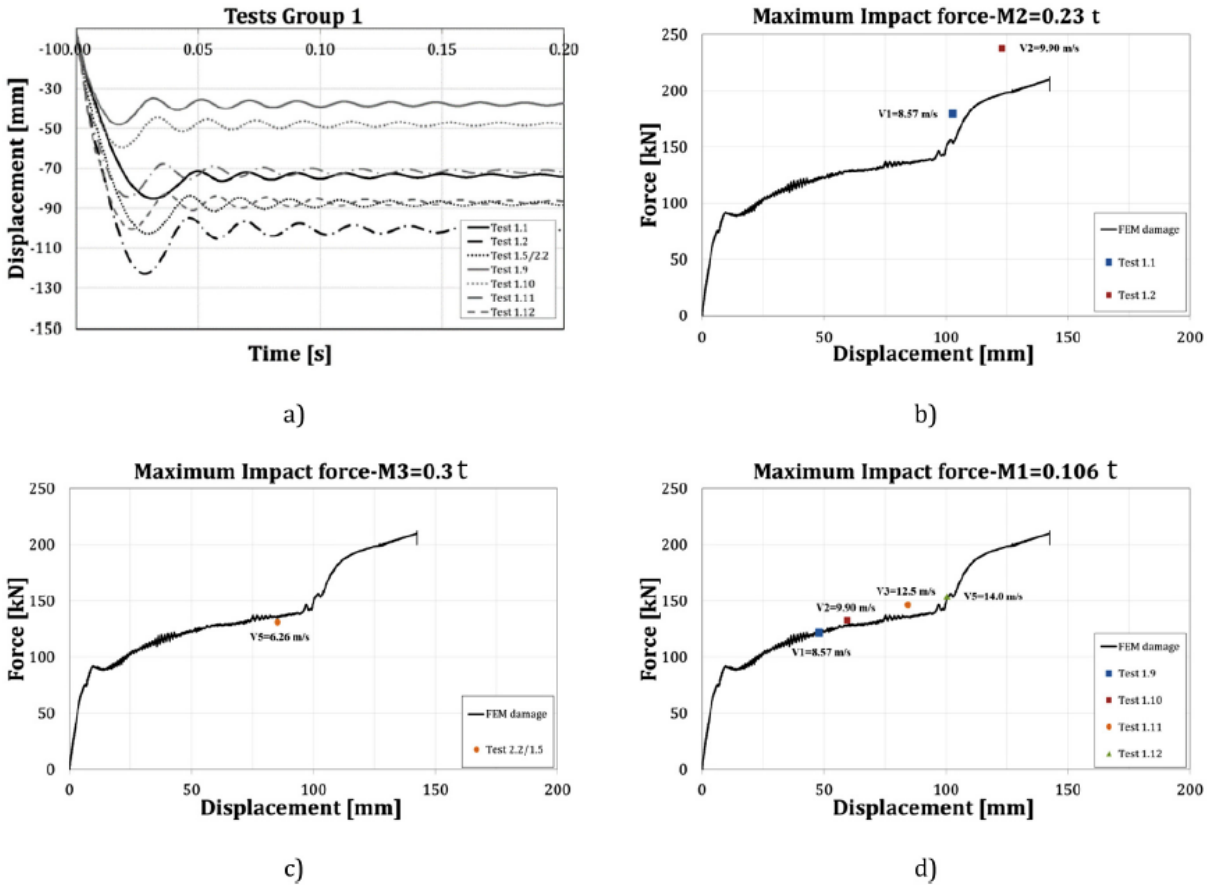

Fig. 20. a) Time-Displacement curve Group 1; b) Static force-displacement curve and impact with M2; c) Static force-displacement curve and impact with M3; d) Static force-displacement curve and impact with M1;

Table 11

Summary of the results.

	Test	M	v	E	F_p	F_{dyn}	d_{max}	d_{perm}	E_{diss}	$F_{st,eq}$	$\dot{\varepsilon}_{max}$	R_E	DIF
	N#	[ton]	[m/s]	[J]	[kN]	[kN]	[mm]	[mm]	[kNmm]	[kN]	[1/s]	[−]	[−]
GROUP 1	1.1	0.23	8.57	8.45E+03	265.48	179.24	103.17	88.5	1.12E+04	153.2	891.7	0.109	1.170
	1.2	0.23	9.90	1.13E+04	329.76	237.67	123.03	100.6	1.61E+04	196.8	2632.4	0.131	1.207
	1.5	0.3	6.26	5.89E+03	292.58	131.21	85.20	74.35	8.98E+03	129.5	326.7	0.105	1.013
	1.9	0.106	8.57	3.89E+03	297.81	121.55	48.1	38.03	4.40E+03	121.2	346.2	0.091	1.003
	1.10	0.106	9.90	5.20E+03	324.71	132.64	59.5	48.59	5.91E+03	128.7	361.5	0.099	1.031
	1.11	0.106	12.53	8.32E+03	332.28	146.62	84.3	71.63	9.31E+03	135.5	332.0	0.110	1.082
	1.12	0.106	14.01	1.04E+04	314.5	153.75	100.5	86.34	1.15E+04	151.9	557.8	0.114	1.012
GROUP 2	2.1	0.23	6.26	4.51E+03	243.15	127.15	65.76	55.7	6.56E+03	129.0	671.9	0.100	0.986
	2.2	0.3	6.26	5.89E+03	292.58	131.21	85.20	73.1	8.98E+03	136.2	326.7	0.105	0.963
	2.3	0.35	6.26	6.87E+03	282.09	147.98	98.02	85.1	1.08E+04	142.1	216.0	0.110	1.041
	2.4	0.4	6.26	7.85E+03	283.09	195.11	107.94	90.8	1.26E+04	175.6	1490.8	0.117	1.111
	2.5	0.45	6.26	8.83E+03	286.68	218.83	116.61	96.9	1.44E+04	192.0	3876.2	0.123	1.140
	2.6	0.5	6.26	9.81E+03	314.98	231.77	124.54	119.7	1.63E+04	197.9	4265.7	0.131	1.171
GROUP 3	3.1	0.23	8.76	8.83E+03	291.35	196.08	107.36	90.8	1.28E+04	174.0	1456.0	0.119	1.127
	3.2	0.3	7.67	8.83E+03	296.41	213.20	111.84	92.8	1.35E+04	186.4	2564.0	0.121	1.144
	3.3	0.35	7.10	8.83E+03	282.16	218.94	113.56	93.7	1.38E+04	188.6	2725.0	0.122	1.161
	3.4	0.45	6.26	8.83E+03	286.68	218.83	116.61	97.5	1.44E+04	192.0	2929.0	0.123	1.140
	3.5	0.5	5.94	8.83E+03	277.50	225.50	124.54	98.3	1.47E+04	198.3	3302.0	0.118	1.137
	3.6	0.55	5.67	8.83E+03	272.19	223.27	119.10	99.1	1.49E+04	194.0	3146.0	0.125	1.151

Published in : Journal of Constructional Steel Research (2022), vol. 192, 107215
DOI: 10.1016/j.jcsr.2022.107215
Status : Postprint (Author's version)

5.2. EFFECT OF THE VARIATION OF THE IMPACT MASS (M)

The second group of parametric tests is considering the influence of the dropping mass weight on the global joint behaviour with a velocity fixed to V_5 = 6.26. Increasing the masses correspond to higher maximum and permanent deformations. However, the impact force varies slower when compared with the impacts of Group 1 (**Fig. 21**). Further increase of the mass (higher than M8 in **Table 9**) leads the bolt failure (in the lower L-stub). As outcome of the Test Group 2 the mass variation has a smaller influence on the joint response than the velocity variation (Group 1 see **Fig. 20**). In fact, in **Fig. 21**, the influence of the dynamic effects are visible only when the mass activates the component in bearing and shear of the connection (after the bolts reach the end stroke of the slotted hole). With M1, M2 and M3 no dynamic effect are visible on the joint response.

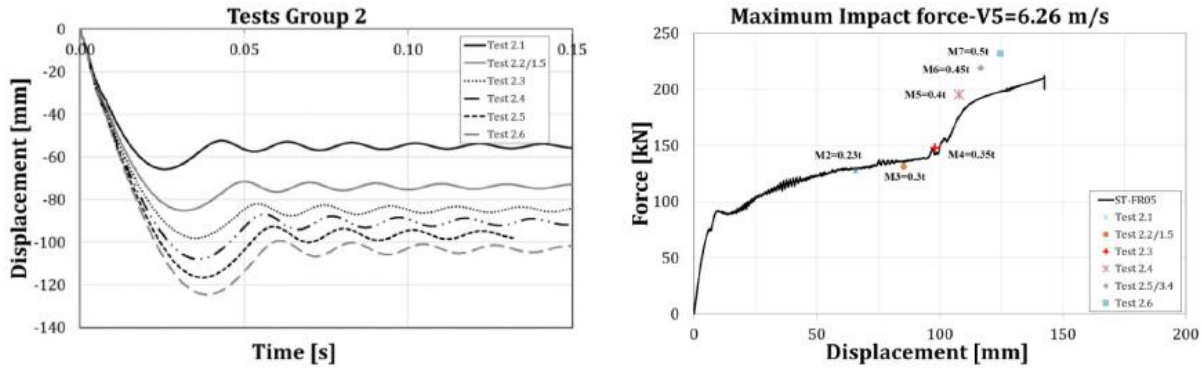

Fig. 21. a) Time-Displacement curve Group 2; b) Static force-displacement curve and impact Group 2.

5.3. EFFECT OF THE CONTEMPORARY VARIATION OF M AND V WITH CONSTANT E

In the third group of parametric investigation, the impact energy is constant during the impacts (equal to E_{11} = 8.87E3 J), while the mass wright and the velocity are varying accordingly. Even though it was clear from the preliminary investigations that energy is the governing parameter, a simultaneous variation of the mass and velocity has reduced influence on the global joint response, this is expected since overall, the energy is governing the dynamic behaviour during an impact. From **Fig. 22** it can be observed that an increase of mass influences slightly more the maximum displacement than the variation of the velocity for a constant value of energy. Nevertheless, the range of investigated velocity is rather small to derive a general behaviour, since a higher speed leads always to joint failure for the investigated geometry. Overall, the joint shows higher impact force but lower maximum displacement compared with the static test, the joint is more resistant but less ductile.

Published in : Journal of Constructional Steel Research (2022), vol. 192, 107215
DOI: 10.1016/j.jcsr.2022.107215
Status : Postprint (Author's version)

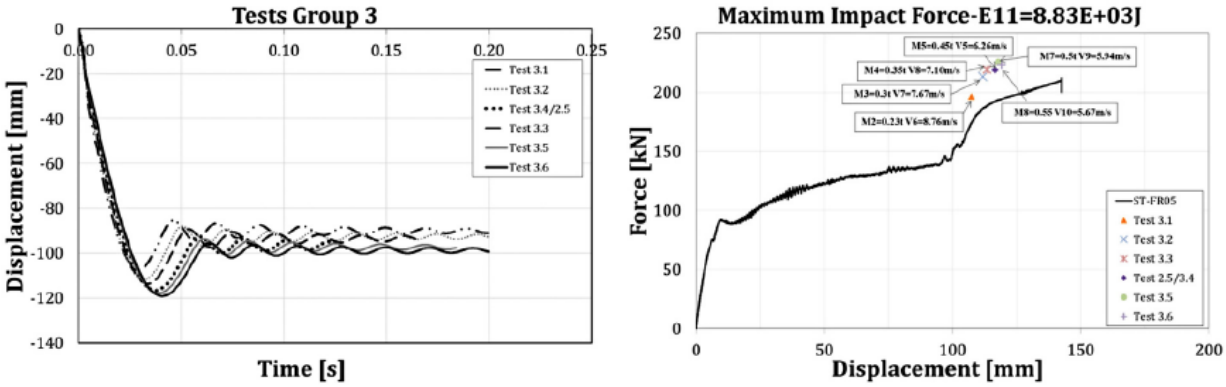

Fig. 22. a) Time-displacement curve Group 3; b) Static force-displacement and impact Group 3.

5.4. ENERGY DISSIPATION RATE (R_E) AND DIFS

The parametric study outcomes are represented with four quantities: impact forces (F_{Dyn}), energy dissipation rates (R_E), maximum displacements (d_{max}) and DIF associated with the performed impacts. The aim is to understand how the behaviour is influenced by the variation of these parameters. The dissipation capacity of the joint, expressed as the integration of the force-displacement, is a function of the deformation capacity. To dissipate more energy, the joint needs to accommodate larger deformations and the relation between the dissipated energy and the displacement is linear (**Fig. 23**a), while the correlation with the maximum dynamic force (**Fig. 23**b) is less evident and harder to generalise.

The energy dissipation rate R_E [36], is a simple way to summarize the overall behaviour of the specimens. It is calculated as follow:

$$R_E = \frac{E_D}{d_{max}} \tag{5-1}$$

where E_D is the energy dissipated by the joint, calculated integrating the force-displacement curves and, d_{max} is the maximum displacement reached under the considered impact. The results of all the performed tests are presented in **Table 11**. Overall, the joint behaviour is governed, as underlined several times, by the impact energy. For a constant value of impact Energy (Group 3), R_E shows minor variations (coefficient of variation of 2% compared with the 12% in other cases). The highest value of the R_E is associated with the two impacts with the highest dissipated energy, for which also the DIF is the highest (Test 1.2 and 2.6). In test 1.1, the high DIF is due to higher strain rate (linked to impact velocity) but the R_E is small due to the smaller energy dissipated.

A small speed (V) increase, even for a small value of the mass (M), is increasing faster the energy dissipation rate due to higher forces associated to strain rate sensitivity (Group 1 in **Fig. 23**c-d).

The DIF is varying from 1.003 to 1.207 (**Table 11**). The highest DIF is associated with the highest tested energy (test 1.2). This is the main difference between impact and static behaviour, which is influenced by the maximum force rather than energy. As a general behaviour, increasing the velocity is increasing the DIF for a fixed value of mass (**Fig. 24**a). However, when the energy is equal to E2 = 1.12E+07 mJ, a

Published in : Journal of Constructional Steel Research (2022), vol. 192, 107215
DOI: 10.1016/j.jcsr.2022.107215
Status : Postprint (Author's version)

higher value of V is always leading to bolt failure (Simulations 1.3–1.4), while, for energy lower than E2, higher values of velocity are always bringing to lower DIFs (test 1.10–1.12).

It is interesting to compare the test 1.11 and 1.12: in test 1.11, the energy is not sufficient to reach the end of the bolt hole stroke, while, in test 1.12, the energy is just sufficient to reach the end of the bolt hole stroke. This means that, for test 1.12, the bolt hits the hole's end but the energy is not sufficient to activate new components. Therefore, even though test 1.11 and 1.12 have the highest velocities, the DIF is lower. In all the other cases (Group 2 and 3 in **Fig. 24**c), there is not a clear correlation between the velocity of impact and the DIF. For Group 2, this is clearly due to a constant velocity while, for Group 3, this is a consequence of a rather constant impact force. The same consideration can be made in term of velocity of rotation of the joint (**Fig. 24**b-d).

The joint seems to resist better to higher velocities than higher masses. In fact, the highest impact force is associated with the highest velocity (Test 1.2), always connected to the strain rate effect. Hoverer, even though the DIF is normally a function of the deformation rate, there is not a clear relation in this case between the rate of deformation (or impact speed of the mass) and the global DIF of the joint. In **Fig. 25**, the evolution of the DIF vs the strain rate for the different groups of the parametric analysis is given. In **Fig. 25**d), the same impact are reported in a logarithmic scale where an exponential correlation can be found (Coefficient of determination 0.6). There is a concentration of impact points in the range of strain rates in between 2500 and 3500 1/s with a DIF varying between 1.12 and 1.21, range of strain rates which can be classified as dynamic impact as these strain rates are higher than 600 1/ s, limit defined in [60]. This difficulty in finding a relation between the global DIF and the strain rate can be easily explained considering different specificities of the studied joint: several complex mechanisms are activated during impact (sliding, behaviour before and after reaching the end of the bolt hole stroke), the three-dimensional distribution of the strain rate, which makes difficult to individuate the correct corresponding value of the strain rate to be used in the correlation. In this work, the strain rates considered in **Fig. 25** correspond to the maximum strain rate values appearing in the specimen during the impact before reaching the maximum displacement. This simplification is quite strong as each joint component presents a different behaviour with a complex distribution of strain rates changing in time and space.

Published in : Journal of Constructional Steel Research (2022), vol. 192, 107215
DOI: 10.1016/j.jcsr.2022.107215
Status : Postprint (Author's version)

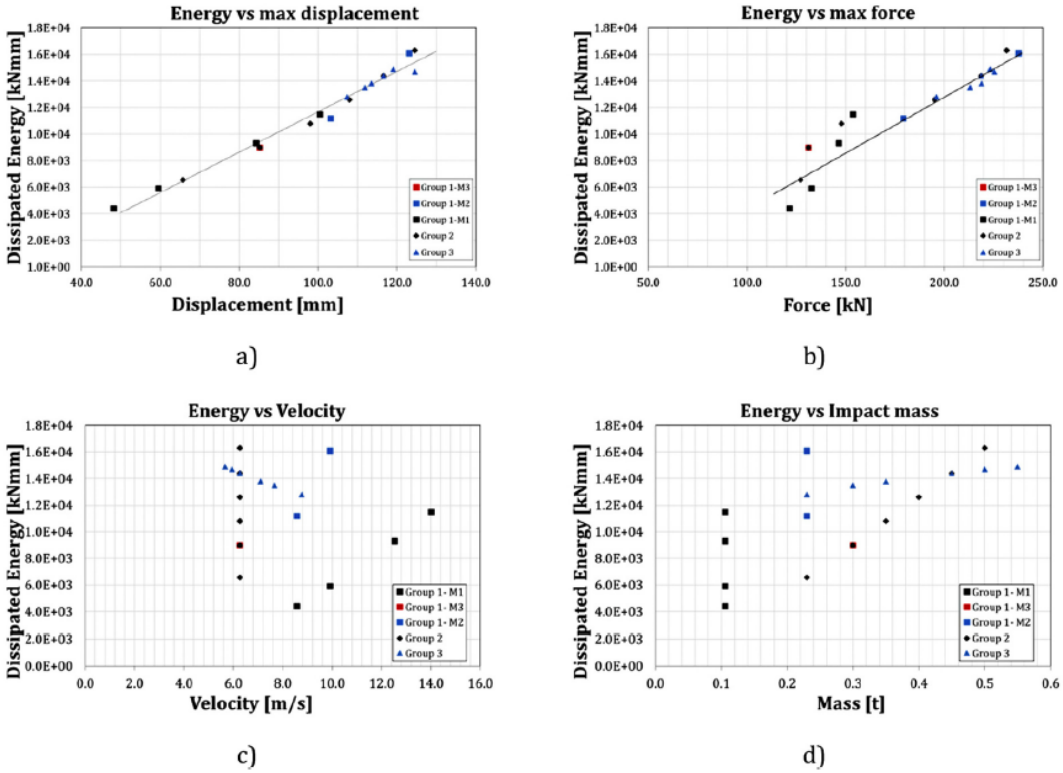

Fig. 23. Evolution of the dissipated energy as a function of the maximum displacement (a), maximum force (b), velocity (c) and dissipated mass (d).

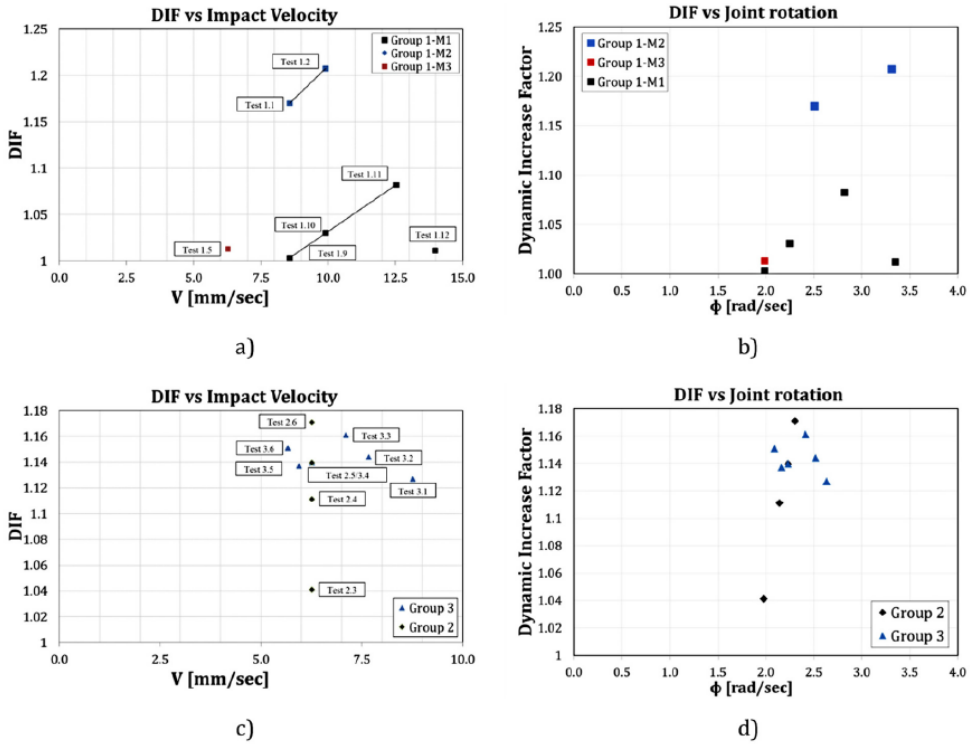

Fig. 24. a) Evolution of the DIF with impact speed Group 1; b) Evolution of the DIF with the velocity of rotation for Group 1; c) Evolution of the DIF with impact speed Group 2-3; d) Evolution of the DIF with the velocity of rotation of the joint for Group 2-3;

Published in : Journal of Constructional Steel Research (2022), vol. 192, 107215
DOI: 10.1016/j.jcsr.2022.107215
Status : Postprint (Author's version)

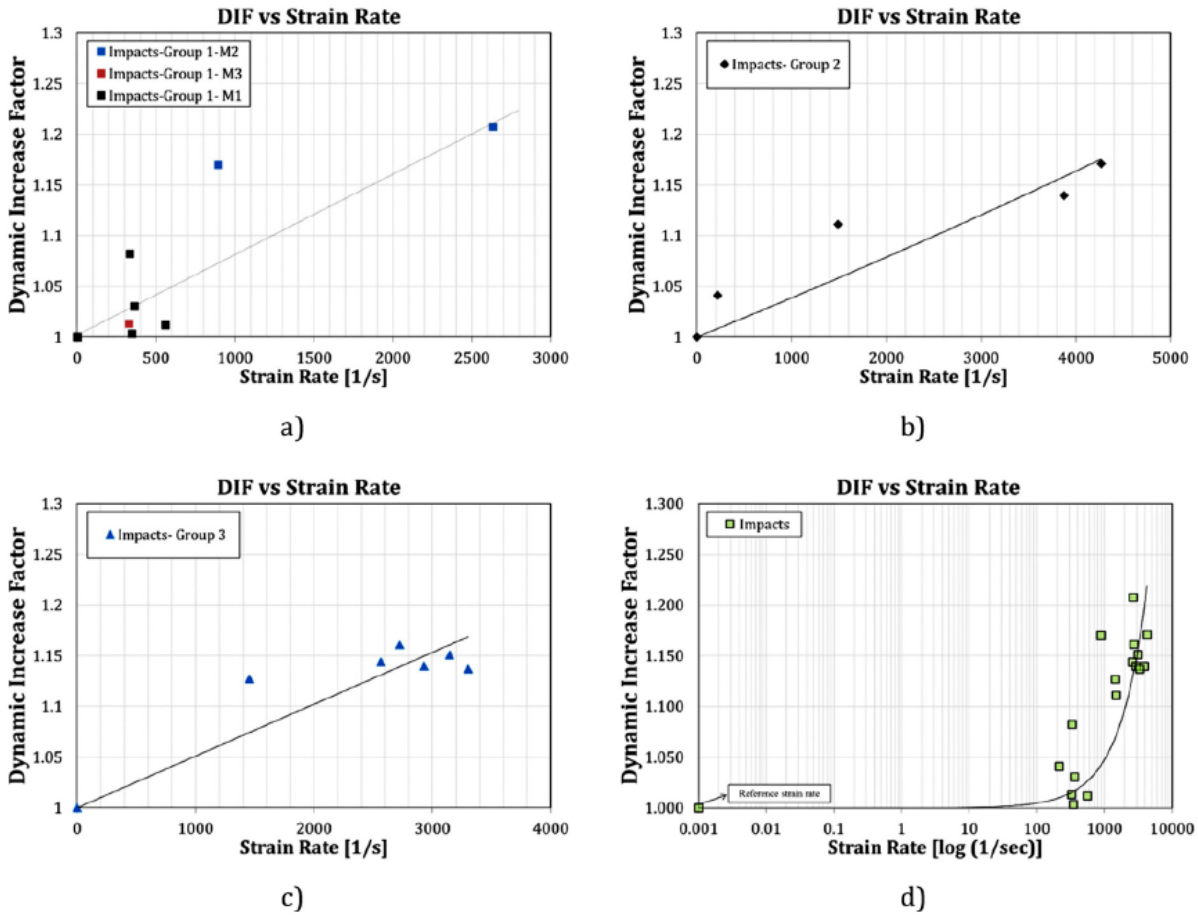

Fig. 25. DIF evolution with the rate of deformation during performed impacts: a) Group 1; b) Group 2; a) Group 3;c) All the impacts vs strain rate in logarithmic scale

6. Conclusions

This work is dealing with the dynamic characterization of SHJs under impact loadings. Drop weight impact tests were performed on a subassembly equipped with double-sided SHJ connections. This characterization has been realized using experimental and numerical approaches. In particular:

- Six impact tests with two different masses have been carried out to characterize the dynamic behaviour of the connection under different impact energies and to calibrate a numerical tool for the development of a parametric study.
- A numerical model was developed in Abaqus/Explicit with 3D brick elements including the calibrated material laws accounting for the strain rate effects and the simulation of material damage up to failure. The model was able to reproduce both the static and the dynamic behaviour of the connection in terms of displacement in time when compared to the experimental results;
- The validated model was then used to perform parametric analyses on the dynamic behaviour of the joint varying the impact mass (M), velocity (V) and impact energy (E). Since the impact resistance is mainly a function of the Energy dissipated rather than the force, R_E (Energy dissipation Rate) associated with each impact has been calculated and used as a parameter of comparison;

Published in : Journal of Constructional Steel Research (2022), vol. 192, 107215
DOI: 10.1016/j.jcsr.2022.107215
Status : Postprint (Author's version)

- The DIFs (Dynamic Increase Factors) were also calculated to characterize the behaviour of these connections under impact when compared to its static response.

The main outcomes of the work can be summarized as follows:

- Increasing V or M increases R_E but, when the impact energy is constant, the joint resists better to higher velocity rather than higher masses due to strain rate effects, even though the investigated velocity range is limited due to the achievement of the bolt failure. The vertical displacement seems to be more sensitive to the drop weight than the velocity;
- There is not a clear correlation between the DIF and the velocity of rotation of the joint because many factors are contributing to a complex velocity distribution in the joint component (velocity, mass and energy of impact);
- The global DIF of the joint does not exhibit a clear correlation with the measured maximum strain rate appearing in the specimen.

Globally, the maximum DIF obtained in the parametric analysis before reaching failure of the joint is 1.2 for the highest impact energy. However, the obtained DIFs are limited to the investigated cases and geometry; more experimental cases on different joint configuration and geometry could improve the results. Finally, in order to try to find a correlation with the joint behaviour and the investigated parameters the experimental tests could include more cases on different geometries.

Declaration of Competing Interest

The authors declare that they have no known competing financial interests or personal relationships that could have appeared to influence the work reported in this paper.

Acknowledgements

The research activity herein presented has been supported by the European Community with the research grant RFSR-CT-2015-00022. The support of the European Commission within RFCS Research & Innovation is gratefully acknowledged. We thank the University of Coimbra for the material tests provided. Particular recognition goes to the technicians of the laboratory of the University of Liège for their precious support and enormous work.

References

[1] M. D'Antimo, Impact Characterization of Innovative Seismically Designed Connections for Robustness Application, University of Liège, 2020.
[2] M. Daie, et al., A new finite element investigation on pre-bent steel strips as damper for vibration control, Int. J. Phys. Sci. 6 (36) (2011) 8044–8050.
[3] n° RFSR-CT-2015-00022, FREEDAM Research Fund for Coal and Steel (RFCS) Research Programme under Grant Agreement, 2022.
[4] C.E. Grigorian, T.S. Yang, E.P. Popov, Slotted bolted connection energy dissipators, Earthquake Spectra 9 (3) (1993) 491, https://doi.org/10.1193/1.1585726.

Published in : Journal of Constructional Steel Research (2022), vol. 192, 107215
DOI: 10.1016/j.jcsr.2022.107215
Status : Postprint (Author's version)

[5] G.C. Clifton, Semi-Rigid Joints for Moment-Resisting Steel Framed Seismic- Resisting Systems, Doctoral thesis, The University of Auckland, 2005.
[6] M.D. Aniello, M. Zimbru, M. Latour, A. Francavilla, Development and Validation of Design Criteria for Free from Damage Steel Joints vol. 1, 2017 no. 2.
[7] M. Latour, V. Piluso, G. Rizzano, Experimental analysis of beam-to-column joints equipped with sprayed aluminium friction dampers, J. Constr. Steel Res. 146 (2018) 33–48, https://doi.org/10.1016/j.jcsr.2018.03.014.
[8] M. Latour, V. Piluso, G. Rizzano, Friction Joints Equipped with Sprayed Aluminium Dampers, no. SEPTEMBER, 2014.
[9] M. Latour, G. Rizzano, Experimental analysis on the cyclic response of beam to column joints: state-of-the-art at Salerno University, Open Constr. Build. Technol. J. 8 (1) (2015) 227–247.
[10] G. Ferrante Cavallaro, A. Francavilla, M. Latour, V. Piluso, G. Rizzano, Experimental behaviour of innovative thermal spray coating materials for FREEDAM joints, Compos. Part B Eng. 115 (2017) 289–299, https://doi.org/ 10.1016/j.compositesb.2016.09.075.
[11] M. Latour, V. Piluso, G. Rizzano, Experimental analysis on friction materials for supplemental damping devices, Constr. Build. Mater. 64 (2014) 159–176.
[12] M. D'Antimo, M. Latour, G.F. Cavallaro, J.P. Jaspart, S. Ramhormozian, J. F. Demonceau, Short- and long- term loss of preloading in slotted bolted connections, J. Constr. Steel Res. 167 (2020), https://doi.org/10.1016/j. jcsr.2020.105956.
[13] S. Gledhill, G. Sidwel, H.H. Khoo, D.C.C.H.H. Khoo, Steel moment frames with Sliding Hinge joints – lessons learnt during implementation, Steel Innov. Conf. 2013 (February) (2013).
[14] L. Kwasniewski, Nonlinear dynamic simulations of progressive collapse for a multistory building, Eng. Struct. 32 (5) (2010) 1223–1235, https://doi.org/ 10.1016/j.engstruct.2009.12.048.
[15] L. Comeliau, B. Rossi, J.-F. Demonceau, Robustness of steel and composite buildings suffering the dynamic loss of a column, Struct. Eng. Int. J. Int. Assoc. Bridg. Struct. Eng. 22 (3) (2012) 323–329.
[16] J.-F. Demonceau, L. Comeliau, J.-P. Jaspart, ROBUSTNESS OF BUILDING STRUCTURES recent developments and adopted strategy, Steel Constr. Des. Res. 4 (3) (2011) 166–170.
[17] ARUP, Review of international research on structural robustness and disproportionate collapse, Dep. Communities Local Gov. (2011) 76.
[18] D. Dubina, F. Dinu, ESsential Features of Robustness Design of Multi-Storey, 2014.
[19] C.C. Segura, L. Hamra, M. D'Antimo, J.-F.F. Demonceau, M. Feldmann, Determination of loading scenarios on buildings due to column damage, Structures 12 (2017) 1–12.
[20] C. Huvelle, V.-L. Hoang, J.-P. Jaspart, J.-F. Demonceau, Complete analytical procedure to assess the response of a frame submitted to a column loss, Eng. Struct. 86 (March) (2015) 33–42.
[21] B.A. Izzuddin, A.G. Vlassis, A.Y. Elghazouli, D.A. Nethercot, Progressive collapse of multi-storey buildings due to sudden column loss — part I: simplified assessment framework, Eng. Struct. 30 (5) (May 2008) 1308–1318.
[22] B. Yang, K. Hai Tan, Robustness of Bolted-Angle Connections against Progressive Collapse: Experimental Tests of Beam-Column Joints and Development of Component-Based Models, 2022.
[23] G. Solomos, S. Kokot, Progressive Collapse Risk Analysis: Literature Survey, Relevant Construction Standards and Guidelines, 2012.
[24] A. Ventura, B. Chiaia, V. De Biagi, Robustness assessment of RC framed structures against progressive collapse, IOP Conf. Ser. Mater. Sci. Eng. 245 (2017), 032033.
[25] B. Yang, K.H. Tan, Numerical analyses of steel beam-column joints subjected to catenary action, J. Constr. Steel Res. 70 (2012) 1–11, https://doi.org/10.1016/j.jcsr.2011.10.007.
[26] J. Ribeiro, A. Santiago, C. Rigueiro, P. Barata, M. Veljkovic, Numerical assessment of T-stub component subjected to impact loading, Eng. Struct. 106 (2016) 450–460, https://doi.org/10.1016/j.engstruct.2015.10.047.
[27] T. Sabuwala, D. Linzell, T. Krauthammer, Finite element analysis of steel beam to column connections subjected to blast loads, Int. J. Impact Eng. 31 (7) (Aug. 2005) 861–876.
[28] E.L. Grimsmo, A.H. Clausen, A. Aalberg, M. Langseth, A numerical study of beam- to-column joints subjected to impact, Eng. Struct. 120 (May) (2016) 103–115.
[29] J. Ribeiro, A. Santiago, C. Rigueiro, Assessment of the T-Stub component subject to high strain-rate, in: Proceedings of the International Conference on Structural Dynamic, EURODYN vol. 2014-Janua, 2014, pp. 3549–3555.
[30] A.F. Santos, A. Santiago, L. Simões, M. Latour, Experimental assessment of friction dampers under impact loading, in: EUROSTEEL, 2017.
[31] R. Rahbari, A. Tyas, J. Buick Davison, E.P. Stoddart, Web shear failure of angle- cleat connections loaded at high rates, J. Constr. Steel Res. 103 (Dec. 2014) 37–48.
[32] H. Kang, J. Shin, J. Kim, Analysis of steel moment frames subjected to vehicle impact, APCOM ISCM (2013).
[33] B. Yang, H. Wang, Y. Yang, S.B. Kang, X.H. Zhou, L. Wang, Numerical study of rigid steel beam-column joints under impact loading, J. Constr. Steel Res. 147 (2018) 62–73.
[34] C. Liu, K. Hai, T. Tat, C. Fung, Dynamic Behaviour of Web Cleat Connections Subjected to Sudden Column Removal Scenario, 2013.
[35] C. Liu, T. Ching Fung, K. Hai Tan, Dynamic Performance of Flush End-Plate Beam- Column Connections and Design Applications in Progressive Collapse, 2022.
[36] H. Wang, B. Yang, X.H. Zhou, S.B. Kang, Numerical analyses on steel beams with fin-plate connections subjected to impact loads, J. Constr. Steel Res. 124 (2016) 101–112, https://doi.org/10.1016/j.jcsr.2016.05.016.
[37] E.L. Grimsmo, A.H. Clausen, M. Langseth, A. Aalberg, An experimental study of static and dynamic behaviour of bolted end-plate joints of steel, Int. J. Impact Eng. 85 (July) (2015) 132–145.
[38] A. Tyas, J.A. Warren, E.P. Stoddart, J.B. Davison, S.J. Tait, Y. Huang, A methodology for combined rotation-extension testing of simple steel beam to column joints at high rates of loading, Exp. Mech. 52 (8) (2012) 1097–1109.

[39] H. Wang, K.H. Tan, B. Yang, Impact resistance of steel frames with different beam–column connections subject to falling-floor impact on various locations, J. Struct. Eng. 147 (4) (Jan. 2021) 04021017.
[40] H. Wang, J. Huo, Y. Liu, N. Wang, M. Elchalakani, Experimental and numerical study on impact behavior of beam-column substructures of steel frame, Structures 29 (Feb. 2021) 14–29.
[41] K. Chen, Y. Zhang, K.H. Tan, Behaviour of steel beam-column joints subjected to quasi-static and impact loads, J. Constr. Steel Res. 183 (Aug. 2021) 106721.
[42] Hamid Sinaei, Evaluation of reinforced concrete beam behaviour using finite element analysis by ABAQUS, Sci. Res. Essays 7 (21) (Jun. 2012).
[43] M.S. Pavlovic, Resistance of Bolted Shear Connectors in Prefabricated Steel- Concrete Composite Decks, 2013, pp. 1–10.
[44] M. D'aniello, D. Cassiano, R. Landolfo, Monotonic and Cyclic Inelastic Tensile Response of European Preloadable gr10.9 Bolt Assemblies, 2016.
[45] M. D'Aniello, D. Cassiano, R. Landolfo, Simplified criteria for finite element modelling of European preloadable bolts, Steel Compos. Struct. 24 (6) (2017) 643–658.
[46] T. Sabuwala, D. Linzell, T. Krauthammer, Finite element analysis of steel beam to column connections subjected to blast loads, Int. J. Impact Eng. 31 (2005) 861–876.
[47] M. D'Antimo, M. Latour, J.-F. Rizzano, Gianvittorio Demonceau, Experimental and numerical assessment of steel beams under impact loadings, J. Constr. Steel Res. 158 (4) (2019) 230–247.
[48] M. D'Antimo, J.-F. Demonceau, M. Latour, Studio di fattibilità sull'utilizzo degli slide hinge joints in strutture resilienti feasibility study on the use of slide hinge joints for resilient structures, Proc. XXVII CTA 2019 (2019).
[49] M. D'Antimo, M. Latour, G. Rizzano, J.-F. Demonceau, J.-P. Jaspart, Preliminary study on beam-to-column joints under impact loading, Open Constr. Build. Technol. J. 12 (1) (2018) 112–123.
[50] CEN, EN 14399–4. High-Strength Structural Bolting Assemblies for Preloading ePart 4: System HV eHexagon Bolt and Nut Assemblies, 2006.
[51] M. D'Antimo, M. Zimbru, M. D'Aniello, J.F. Demonceau, J.P. Jaspart, R. Landolfo, Preliminary finite element analyses on seismic resistant FREE from DAMage beam to column joints under impact loading, Key Eng. Mater. 763 (Feb. 2018) 592–599.
[52] M. D'Antimo, J.-F. Demonceau, M. Latour, G. Rizzano, J.-P. Jaspart, 03.11: experimental investigation of the creep effect on prestressed bolts used in innovative friction connections, ce/papers 1 (2–3) (Sep. 2017) 580–589.
[53] M. D'Antimo, M. Latour, G.F. Cavallaro, J.-P. Jaspart, S. Ramhormozian, J. Demonceau, Short- and long- term loss of preloading in slotted bolted connections, J. Constr. Steel Res. 167C (2020).
[54] M. Bäker, How to Get Meaningful and Correct Results from Your Finite Element Model, 2018, pp. 1–26.
[55] M. D'Aniello, R. Tartaglia, S. Costanzo, R. Landolfo, Seismic design of extended stiffened end-plate joints in the framework of Eurocodes, J. Constr. Steel Res. 128 (2017) 512–527.
[56] M. D'Aniello, M. Zimbru, R. Landolfo, M. Latour, G. Rizzano, V. Piluso, Finite element analyses on free from damage seismic resisting beam-to-column joints, in: COMPDYN 2017 - Proceedings of the 6th International Conference on Computational Methods in Structural Dynamics and Earthquake Engineering vol. 1, 2017, pp. 802–814, no. June.
[57] M. D'Antimo, M. Latour, J. Jaspart, J. Demonceau, Numerical and experimental investigation of simply supported steel beams under drop-weight impact tests, ce/ papers 3 (3–4) (Sep. 2019) 803–809.
[58] W.S. Lee, C.F. Lin, Impact properties and microstructure evolution of 304l stainless steel, Mater. Sci. Eng. A 308 (2001) 124–135, https://doi.org/10.1016/S0921- 5093(00)02024-4.
[59] G. Culache, M.P. Byfield, N.S. Ferguson, A. Tyas, Robustness of beam-to-column end-plate moment connections with stainless steel bolts subjected to high rates of loading, J. Struct. Eng. (United States) 143 (6) (2017), https://doi.org/10.1061/ (ASCE)ST.1943-541X.0001707.
[60] J. Ribeiro, A. Santiago, C. Rigueiro, L.S. Da Silva, Analytical model for the response of T-stub joint component under impact loading, J. Constr. Steel Res. 106 (2015) 23–34.
[61] E. Elettore, F. Freddi, M. Latour, G. Rizzano, Design and analysis of a seismic resilient steel moment resisting frame equipped with damage-free self-centering column bases, J. Constr. Steel Res. 179 (2021), https://doi.org/10.1016/j. jcsr.2021.106543.
[62] A. Lemos, L.S. Da Silva, M. Latour, G. Rizzano, Numerical modelling of innovative DST steel joint under cyclic loading, Arch. Civil. Mech. Eng. 18 (3) (2018) 687–701.
[63] T. Gernay, A. Gamba, Progressive collapse triggered by fire induced column loss: detrimental effect of thermal forces, Eng. Struct. 172 (2018) 483–496, https://doi. org/10.1016/j.engstruct.2018.06.060.